Final Report

DEVELOPMENT OF A TURBIDITY-MEASURING UNDERWATER OPTICAL RADAR SYSTEM

By: K. S. KRISHNAN W. E. EVANS
R. C. HONEY G. P. SORENSON

Prepared for:

OFFICE OF NAVAL RESEARCH
DEPARTMENT OF THE NAVY
WASHINGTON, D.C. 20360

SRI
STANFORD RESEARCH INSTITUTE
Menlo Park, California 94025 · U.S.A.

72

STANFORD RESEARCH INSTITUTE
Menlo Park, California

Final Report *December 1969*

DEVELOPMENT OF A TURBIDITY-MEASURING UNDERWATER OPTICAL RADAR SYSTEM

By: K. S. KRISHNAN W. E. EVANS
R. C. HONEY G. P. SORENSON

Prepared for:

OFFICE OF NAVAL RESEARCH
DEPARTMENT OF THE NAVY
WASHINGTON, D.C. 20360

CONTRACT N00014-68-C-0450

SRI Project 7325

Approved:

RAY L. LEADABRAND, *Executive Director*
Electronics and Radio Sciences

Copy No. 33

ABSTRACT

The results of a feasibility study of measuring subsurface turbidity in the ocean are presented. The design and development of the laser transmitter and receiver packages of an underwater optical radar system are discussed. The initial performance of the equipment in three field trials in the Pacific Ocean is described, the data obtained is discussed, and the system is evaluated.

FOREWORD

The research program discussed in this report was conducted under Contract No. N00014-68-C-0450, NRL Reqn. 00173-8-006305/4-25-68, sponsored by the Office of Naval Research, Department of the Navy, Washington, D.C. The project monitor was Dr. Frank C. Macdonald of the Naval Research Laboratory, Washington, D.C.

The research covered the period from 1 June 1968 till 31 August 1969. The project supervisor, Dr. R. C. Honey, was responsible for the research activity under SRI Project 7325.

CONTENTS

ILLUSTRATIONS

TABLES

ACKNOWLEDGMENTS

The authors acknowledge with gratitude the contributions of Mr. Curtis H. Roché in the design and fabrication work, as well as the conduct of the experiments; and those of Mr. John A. Hudick in the fabrication of the receiver. The authors are indebted to Dr. Arthur Vassiliadis, Mr. Norman Peppers, and Mr. Arne Rosengreen for many valuable discussions.

I INTRODUCTION

The principal objective of the research program is to demonstrate the usefulness of an optical radar system for measuring the temporal and spatial characteristics of turbidity clouds and layers in the ocean. These characteristics are of too fine a scale to be measured in three dimensions by means other than optical ranging systems. Such information is necessary for evaluating the feasibility and false-alarm characteristics of any proposed turbidity-wake detection technique or system.[1]* Apart from these needs, information on the structure of turbidity in the sea is of considerable usefulness to marine biologists, to investigators of underwater visibility and in furthering general understanding of the ocean environment.

This report describes the program of work that developed the optical radar (lidar) system for underwater use. A Q-switched Neodymium-doped glass laser whose output is frequency doubled with a potassium dihydrogen phosphate (KDP) crystal has been developed for transmitting a light beam under water in a wavelength range having near-minimum attenuation. A sensitive receiver of reasonable size to collect the scattered returns from the transmitted pulse has been designed along with a data handling and display system capable of handling the high speeds and the expected large amplitude range of the returns. The development of the transmitter and receiver packages are described in detail.

In addition to testing the system under laboratory conditions, it was tested in the Pacific Ocean on three occasions. New problems arose during each of these field trials, with valuable experience and insight

---

*References are listed at the end of the report.

gained in overcoming them. These are described and the data obtained are presented and discussed at length.

Finally, future avenues of work that will lead to the fulfillment of the initial goals of the program are briefly presented.

II UNDERWATER LIDAR TRANSMITTER

A. General Considerations

In the design of a laser system to transmit a light beam under water, the high attenuation of light in water dominates all system considerations for all wavelengths; however, wavelengths in the vicinity of 500 nm suffer the least attenuation.[2] In order to maximize the range of the lidar system, the laser source should be in this wavelength range. Such a source is conveniently obtained by frequency-doubling a Neodymium laser whose fundamental output is at 1062 nm. The second harmonic at 531 nm obtained with a nonlinear crystal such as KDP (potassium dihydrogen phosphate), would have an attenuation coefficient of 0.042 per meter, or 0.18 dB/m, in pure water.[3]

This means that all the photons in a 10-millijoule pulse at this wavelength would be absorbed or scattered, leaving only a single unscattered photon, at a range of about 350 meters; and, for a 10-joule pulse, only a single unscattered photon would remain at a range of about 500 meters.

Thus, even in pure water, the ranges available are not very large. In ocean waters under practical lidar operating conditions the return ranges are expected to be in the neighborhood of 10 to 50 meters, depending on the clarity of the water. Increasing the pulse energy by an order of magnitude results in a relatively small increase in range. Considering the design characteristics of the receiving system together with the laser system, it was decided that a 10-ns pulse at 530 nm with an energy of 10 millijoules would be adequate for the purposes of this study. The laser system performance was directed to this criterion.

One of the initial objectives on this program was that a minimum amount of money would be spent on the laser to be used for these studies; hence arrangements were made to secure the loan of an RCA-built doubled-Nd-glass laser system in an underwater housing. Unfortunately, this system, as supplied, had a history of mechanical, electrical, and optical problems that required a very considerable amount of time and effort to resolve. The present laser bears little resemblance to the original but is still not an optimum system for the underwater lidar application. For instance, the use of Nd-doped-glass results in a very much wider spectral output from the laser than can be obtained from Nd-doped YAG. This results in reduced system range when the backscattered return must compete with ambient background light in the receiver.

B. Description of the Laser System

The present configuration of the laser is shown in Figures 1 through 4. The optical cavity is formed by a high-quality quartz, totally internally reflecting (TIR) prism at one end, and a high-reflectivity (87 percent peak) etalon (resonant reflector) consisting of three z-axis cut sapphire flats. The laser rod is 1/4 inch in diameter, and 3 inches long. It is a silicate glass (Owens-Illinois designation ED-2) doped with Neodymium to a concentration of 3 percent. The two ends of the rod are flat and parallel but are not coated. Both the laser rod and a Xenon flash lamp for pumping are housed in an elliptical reflecting cavity, which is forced-air-cooled with a blower. Q-switching is performed by a rotating prism driven at about 24,000 rpm by a 24-volt dc motor. A magnetic pickup mounted on the prism assembly serves to time the laser pulse with respect to the pumping flash. A quartz plate mounted at the Brewster angle increases the loss of one polarization and thus polarizes the 1062 nm laser output in the orthogonal polarization. Such polarization is necessary for efficient second-harmonic generation under phase-matched

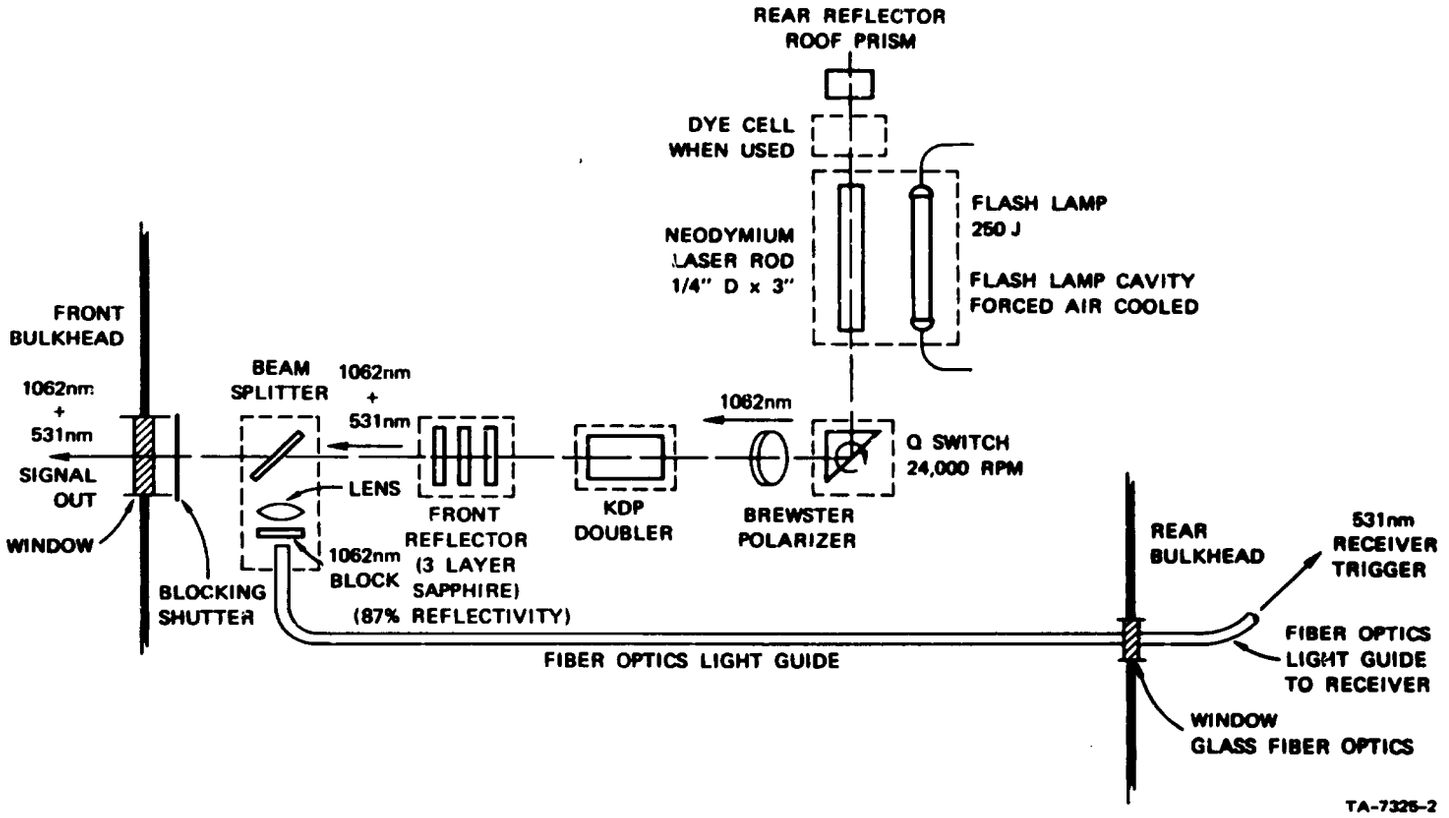

FIGURE 1 DIAGRAM SHOWING OPTICAL SYSTEM OF LASER TRANSMITTER

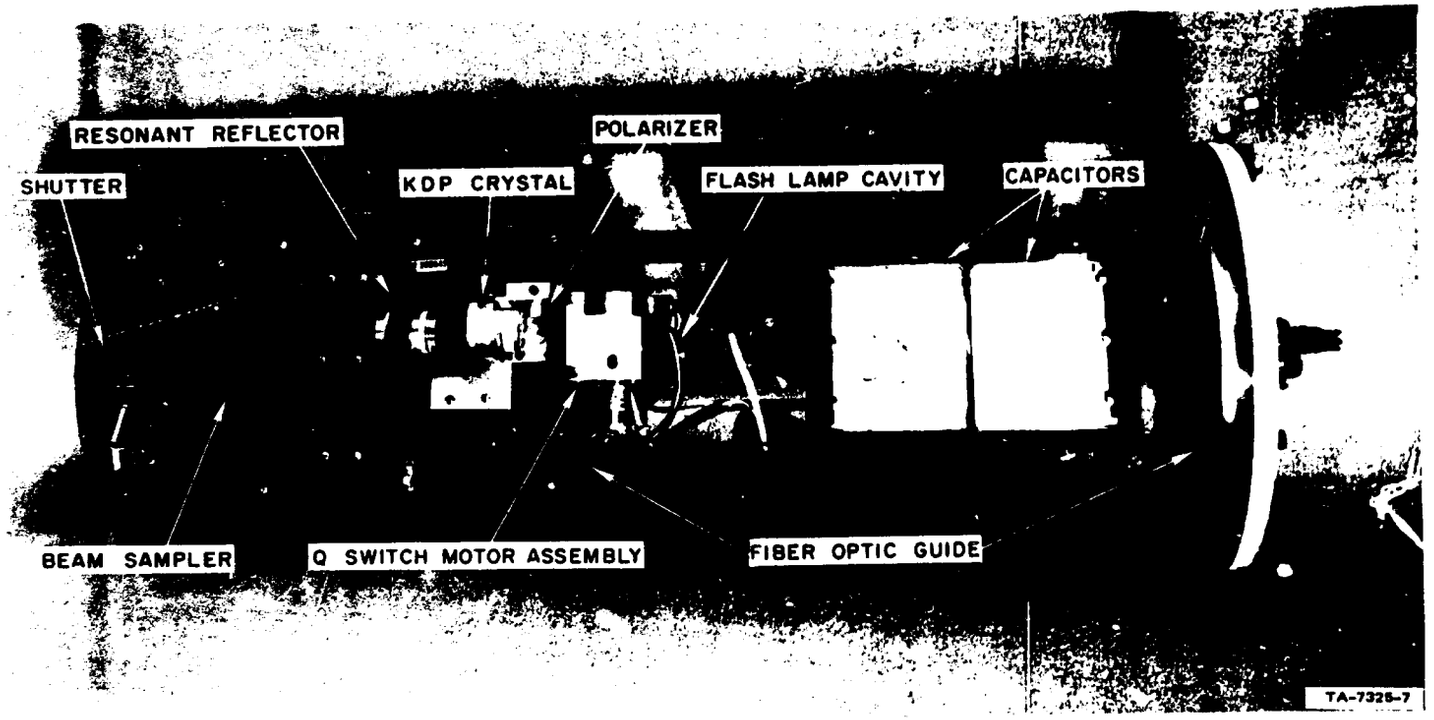

FIGURE 2 LASER TRANSMITTER SHOWING OPTICAL SYSTEM

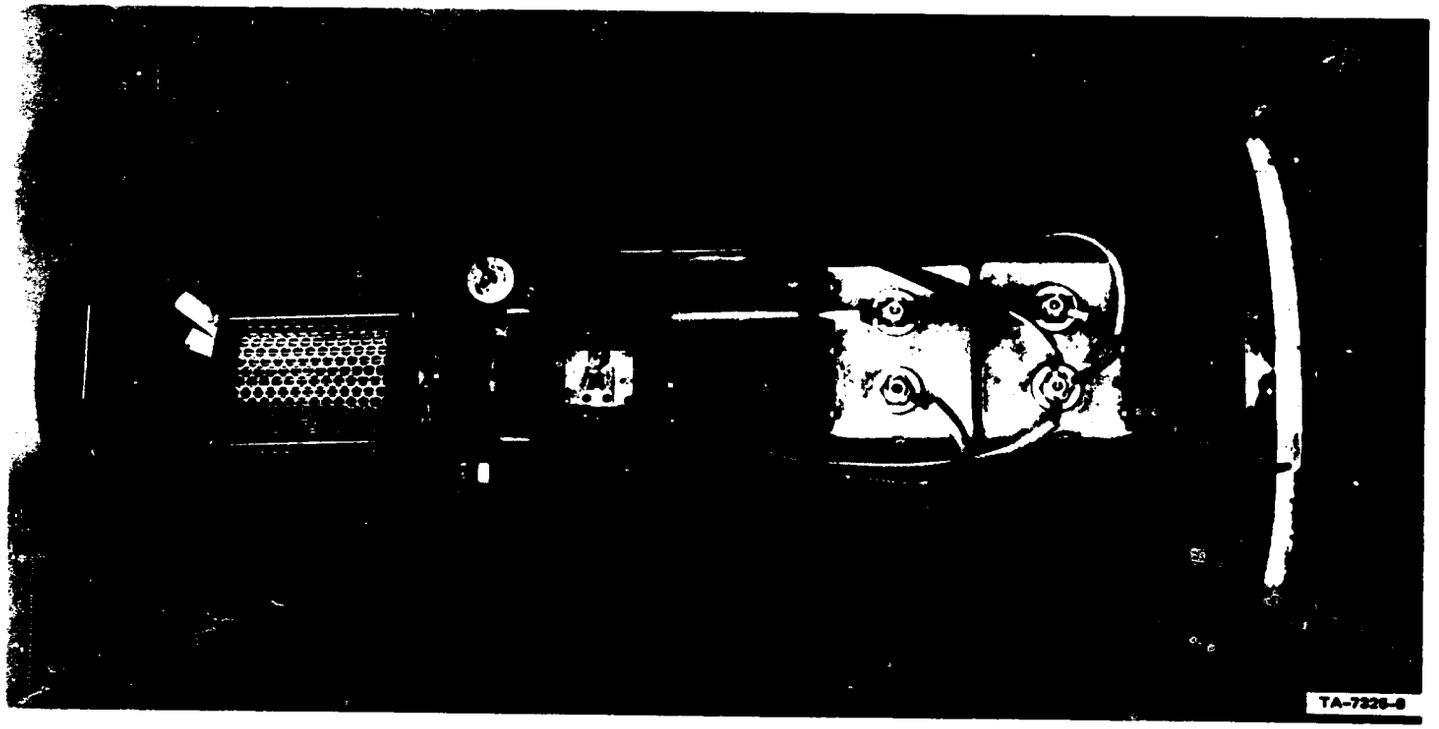

FIGURE 3 LASER TRANSMITTER SHOWING ELECTRICAL SYSTEM

FIGURE 4 LASER TRANSMITTER SHOWING BULKHEAD CONNECTIONS

conditions. The nonlinear crystal used inside the cavity for frequency doubling is potassium dihydrogen phosphate (KDP). It has been cut at the proper orientation to produce 531 nm (green) radiation and packaged suitably in a cell to prevent deterioration due to humidity. The output of the cavity thus consists of the wavelengths 1062 nm and 531 nm at orthogonal polarizations.

Provision has been made to allow a glass cell (cuvette) containing a saturable dye solution to be placed adjacent to the TIR prism for shortening the pulse.

A beamsplitter provides a sample of the output of the cavity. The 1062-nm radiation is filtered out and the 531-nm radiation is attenuated and focused into a fiber optic guide to be used for triggering the receiver package.

While a 1062-nm (block) filter is used for laboratory experiments, the high absorptivity of water (56.4 dB/m)[4] is depended upon, to remove the 1062-nm component of the transmitter output. The solenoid-activated blocking shutter is provided to block the output while allowing the rest of the system to function in order to facilitate testing, trouble shooting, and interference-tracing.

The optical components are mounted on a rigid aluminum frame. The electrical components--namely, the energy storage capacitors and the triggering electronics as well as the recirculating air cooling system--are also mounted on this frame. The complete transmitter package is housed in a watertight enclosure consisting of a 9-inch-diameter, 32-inch-long flanged aluminum pipe. A window is provided for the output laser beam on one flange, and the electrical and optical connections are made at the other.

Without the nonlinear crystal, the laser system is capable of producing 1062-nm radiation in the range of 0.2 joule per pulse with

an input energy of 120 joules to the flash lamp. The pulse lengths are on the order of 15 to 18 nanoseconds. A pulse-repetition rate as much as once in 5 seconds has been used. This rate is limited only by the time taken by the capacitor to charge through a ferro-resonant transformer.

With the nonlinear crystal inside the laser cavity, the laser produces about 15 millijoules of 531-nm radiation and about 0.15 joule of 1062-nm radiation with an input of about 300 joules to the flash lamp. The pulse length of the 531-nm radiation is about 12 to 15 nanoseconds, which is shorter than the corresponding 1062-nm radiation by a few nanoseconds. The use of a low concentration (~1 percent) of a saturable dye in the cuvette results in a shortening of both pulses. Pulse lengths on the order of 8 to 10 nanoseconds for the 531-nm radiation have been achieved by this means. Typical pulse shapes are shown in Figure 5.

The 1062-nm and the 531-nm beam sizes are about 1/4-inch in diameter at the exit of the laser package. The angular divergence of the 531-nm beam is small (~2 minutes of arc) in the plane containing the axis of the spinning prism, but is about 1/2 degree in the plane at right angles to it. The orientation of this fan-shaped beam is at an angle of 16° to the center lines of the two packages.

The parameters related to the performance of the laser are summarized in Tables I and II.

C. Evolution of the Laser System

The initial problems with the laser system as received by Stanford Research Institute (SRI) had to do with the inability of the optical components to handle the high power levels in the cavity. The dielectric mirrors used originally had a very short operating life. The glass laser rod had a plano-TIR design and the edge of the prismatic end was easily

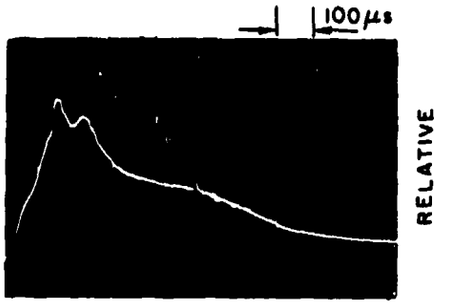

(a) LASER PULSE SUPERIMPOSED ON FLASH LAMP OUTPUT

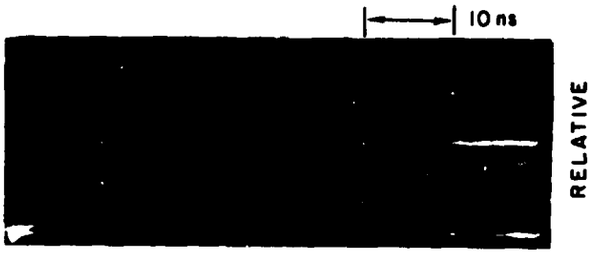

(b) LASER TRANSMITTER OUTPUT AT 1062 nm FWHM 18 ns

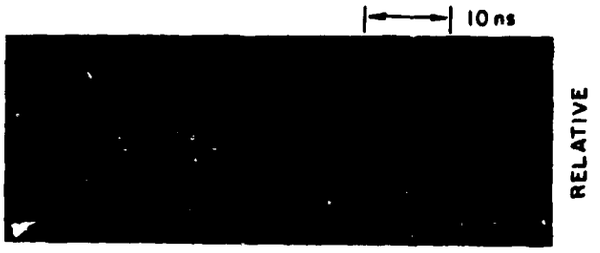

(c) LASER TRANSMITTER OUTPUT AT 531 nm FWHM 14 ns

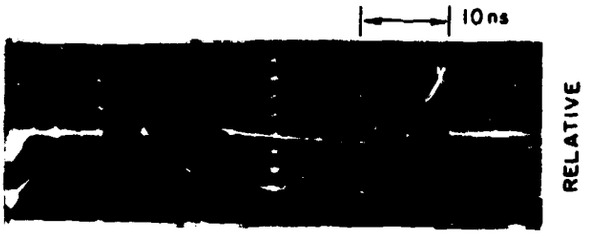

(d) LASER TRANSMITTER OUTPUT AT 531 nm FWHM 9 ns

TA-7325-10

FIGURE 5 TYPICAL FLASH LAMP AND LASER PULSES

Table I

LASER CHARACTERISTICS

Laser host material	Owens-Illinois ED-2 silicate glass
*Neodymium concentration:	3.1 percent by weight ($= 2.83 \times 10^{20}$ Nd ions/cc)
Theoretical maximum laser output $[(nh\nu)/2]$	63.93 joules
*Center of lasing wavelength	1062.3 nm
*Fluorescent line width	26.0 nm

*Information supplied by manufacturer.

Table II

LASER PERFORMANCE PARAMETERS

Parameter	Value at	
	1062 nm	531 nm
Pulse energy (joules)	0.15	0.015
Normal pulse width (ns)	15-18	12-15
Pulse width with 3/4 percent solution of dye (ns)	13-15	8-10
Peak power (MW)	≈10	≈1
Beam diameter (inch)	1/4	1/4
Beam divergence (deg x minutes of arc)	1/2 x 2	1/2 x 2
Attenuation in water (dBm^{-1})	56.4	0.18

damaged. To eliminate these difficulties, the mirror was replaced by the sapphire resonant reflector, and the laser rod was changed to a plano-plano rod with the addition of a fused-quartz roof prism. Further, provision was made to cool the flash-lamp cavity with forced air to reduce thermal effects and increase the pulse-repetition rate.

Various electrical modifications were made, among them the following. The high-voltage supply used to charge the capacitors was made external and a ferroresonant transformer was used to supply a constant charging current. A beam-sampling photodiode was substituted with a fiber-optic guide leading to a PIN diode in the receiver package.

The initial experience with the resonant reflector was quite satisfactory and the end mirror was no longer a limitation to power-handling abilities. However, as further experience was gained with the reflector as a component in the cavity, it was found to have polarizing properties, though the sapphire flats in the component were to have been cut with the z-axis (optic axis) normal to the flats. Thus, inserted between crossed polarizers the etalon caused transmission zeros on rotation through every 90°.

When it was found that this effect interfered with the efforts to polarize the beam with a polarizer in the cavity, a replacement was procured. However, the latter was also found to have polarizing properties, though to a somewhat smaller degree. When it was found that a third etalon available in the laboratory also had similar properties, it was decided to accept this property and mount the reflector at a rotational position experimentally found to give optimum performance. A further curious property of the etalon was accidentally discovered while trying to optimize the output. It was found that if the etalon was moved off normal alignment by a few minutes of arc, the cavity output increased considerably. No explanation for this behavior has

been found except that it might be counteracting the effect of the error in the orientation of the flats.

The nonlinear crystal that was originally in the system was an unprotected potassium dihydrogen phosphate crystal that had deteriorated with time. When it was sent to be repolished and mounted in a protective cell, it was damaged by the supplier. A new crystal mounted in a protective cell was obtained. On using this crystal, it was determined that the crystal was not of the proper crystallographic orientation for phase matching, and no second-harmonic generation was possible. Other techniques for testing the crystallographic orientation were hampered by the packaging of the crystal. A replacement was obtained and was almost immediately successful in second-harmonic generation. It has now functioned effectively over a long period of time and is a reliable component.

Another source of problems with the system has been the rotating prism Q-switch assembly. Initially, the surfaces of the prism were anti-reflection-coated and these failed rapidly. Further, due to inexact alignment of the rotation axis and the reflecting surface of the prism, the laser beam damaged the prisms. It was also found that stress-free mounting of the prism was necessary for good laser performance. When these faults were corrected, the troubles with the prism were overcome.

However, continuing uncertainty exists about the motor driving the prism. This 24,000-rpm 24-volt dc miniature motor is run under almost no load conditions. Under these conditions, the speed of any one motor fluctuates by more than 2 percent, and the speed variations from unit to unit are as much as 10 percent. This causes a change in the timing of the system as the speed wanders, contributing to some irregularities in the laser output from shot to shot. Replacement of motors necessitates retiming of the system. The program has also been affected by the

untimely failures of several of these motors after a few hours of operation. These failures begin as larger than normal variations in the speed of the motor as evidenced by the pitch, finally resulting in the seizure of the bearing. Some of these failures have been tentatively traced to dust from the brushes finding their way into the sealed bearings of the motor. The potential problem continues to exist in the present system in spite of the use of special brushes recommended by the manufacturer. A related question is the pulse width of the laser output. With motors whose speeds were near 24,000 rpm, 1062-nm pulse lengths on the order of 13 to 15 ns were obtained, while with motors of the lower speed of 22,000 rpm the pulse lengths increased to 15 to 18 ns. Thus the motor is undeniably a weak link in the present system.

When the initial system was assembled with the 1062-nm output of the cavity passing through the externally mounted KDP crystal, the output at 531 nm was minimal. The best performance produced only about 10^{-3} joule of 531-nm radiation with about 0.1 joule of 1062-nm radiation from the cavity. Several modifications were tried, to improve the conversion efficiency.

The first was to polarize the 1062-nm beam so that the 1062-nm fundamental beam could be sent in as the ordinary ray in the KDP (a negative uniaxial crystal), since the orthogonal polarization would be ineffective in second-harmonic generation. This was accomplished by mounting a quartz flat at the Brewster's angle inside the cavity. Almost complete polarization of the 1062-nm beam was achieved after the effects of the resonant reflector were noted and suitable measures taken as outlined earlier.

It was observed early in the program that the laser output had a relatively large divergence in one plane. The KDP was now mounted such that this divergence occurred in the less critical plane for the crystal--

i.e., the beam divergence was normal to the optic axis of the crystal. An increase in the conversion efficiency was observed after these measures, leading to a few millijoules of output at 531 nm.

Focusing of the beam to reduce the diameter from 1/4 to 1/16 inch where it traversed the KDP was next attempted. An increase in the second-harmonic generation to 5 to 6 millijoules was observed. However, due to the limitations of space and the difficulties due to the packaging of the KDP, it was not possible to use this configuration.

Harder pumping was next attempted, but even at high levels the second-harmonic energy was not adequate. In addition, it was found that beam divergence got worse at higher pumping levels. With such high-reflectivity mirrors in the cavity, the energy density in the laser rod and other optical components was also causing concern. This suggested that advantage should be taken of this high energy density inside the cavity by situating the KDP crystal there. After such a modification, the initial source of concern was the optical quality of the packaging of the KDP, which would determine the energy levels it could handle.

Hence, starting with low pumping levels, the cavity output at both wavelengths was monitored. It was found that the threshold increased considerably due to the additional losses, and that all the components required more critical adjustment with the crystal inside the cavity. Fortunately, the conversion efficiency was superior to previous performance at even small pumping levels above threshold. The crystal has performed well ever since and has not shown any degradation at the highest pump levels that have been used. About 15 millijoules of output at 531 nm has been consistently observed.

It was realized that in this method the higher the reflectivity of the end mirrors, the greater was the energy density in the cavity, and thus the second-harmonic generation would be higher. However, the

resonant reflector, being a wide-band reflector, transmits out of the cavity only a small percentage of the generated second-harmonic radiation. It is also conceivable that the reflected second harmonic can cause the tail of the laser pulse to be long, since Nd^{+3} exhibits strong absorption at about 530 nm. A dispersive mirror that is transparent at the lower wavelength would permit the use of all the second harmonic generated. Such mirrors are difficult to make and fragile in use at high power levels. An alternative system was set up in an attempt to increase the second-harmonic output. Since the fundamental and second harmonic are of orthogonal polarizations, it is possible to separate them with a Glan-Thomson prism. Further, the prism would also serve as a polarizer. Thus, a Glan-Thomson prism was used to replace the polarizing plate in the cavity. The experiment was successful to the extent that it removed the second harmonic effectively from the KDP output. However, the losses caused in the desired polarization of the 1062-nm radiation by the prism increased the threshold to unacceptable levels. A special design of the prism would have reduced these losses; however, this avenue was not pursued since the power levels obtained (~1 MW peak power) were considered sufficient for field tests at this stage.

As mentioned earlier, the pulse length of the laser output at this stage was 12 to 15 ns. For the present use, this pulse length was considered longer than desirable. After experimentation with all the optical components it was found that no improvement could be effected. The only alternatives left were a faster rotation of the Q-switching prism or the use of a saturable absorber to shorten the pulse. Since the former would have involved substantial design changes in the system, the latter was attempted. Eastman Q-switch solution 9740, which has been fairly successful with Nd lasers, was used. By experimentation it was found that a 3/4 percent solution of the as-received dye in chlorobenzene used in a 1-cm-path-length cuvette in the laser cavity (in

addition to the Q-switching prism) led to pulsewidths on the order of 8 ns, which was judged adequate for use, even though the threshold for operation went up considerably.

Other problems also arose in this investigation. Aside from the initial higher threshold, it was found that the dye deteriorated after about a hundred shots, producing a blue stain on the inside of the cuvette at the position of the laser beam, thus effectively limiting the use of a dye cell to about 100 shots. In addition, the dye solution was found to have a "half-life" of about three months. In other words, after three months, twice as concentrated a solution was needed for the same task. Further, with age, the "blue stain" appeared with fewer shots and the usefulness of a batch of dye solution was thus considerably reduced. For these reasons, it was decided to use the dye in the field tests only under conditions where the shorter pulse lengths obtainable with the dye were imperative.

III UNDERWATER LIDAR RECEIVER

A. Design Objectives

The design objectives for the receiver of the underwater lidar system were as follows:

(1) To obtain the maximum sensitivity consistent with a reasonably sized collection aperture

(2) To employ both amplitude-dependent and time-dependent video gain compression techniques in order to be able to display as large a range of video signal amplitudes as possible

(3) To have sufficient bandwidth and display writing speed to be compatible with laser pulse durations of 10 ns or less

(4) To provide for quantitative calibration of each return relative to the level of the transmitted pulse

(5) To have remote (from the deck) control of all critical receiver parameters, including field-of-view.

B. Physical Layout

The major components of the receiver are visible in Figures 6 and 7. The simple plano-convex collecting lens is 10 inches in diameter, with a 9-inch-diameter clear collecting area. It is strong enough to serve as a window as well as focusing lens to depths of at least 100 feet. In the focal plane of the lens is a remotely controlled disc containing four field-stop apertures that determine the field of view of the receiver. The physical size of these apertures and the corresponding viewing angles are tabulated in Table III.

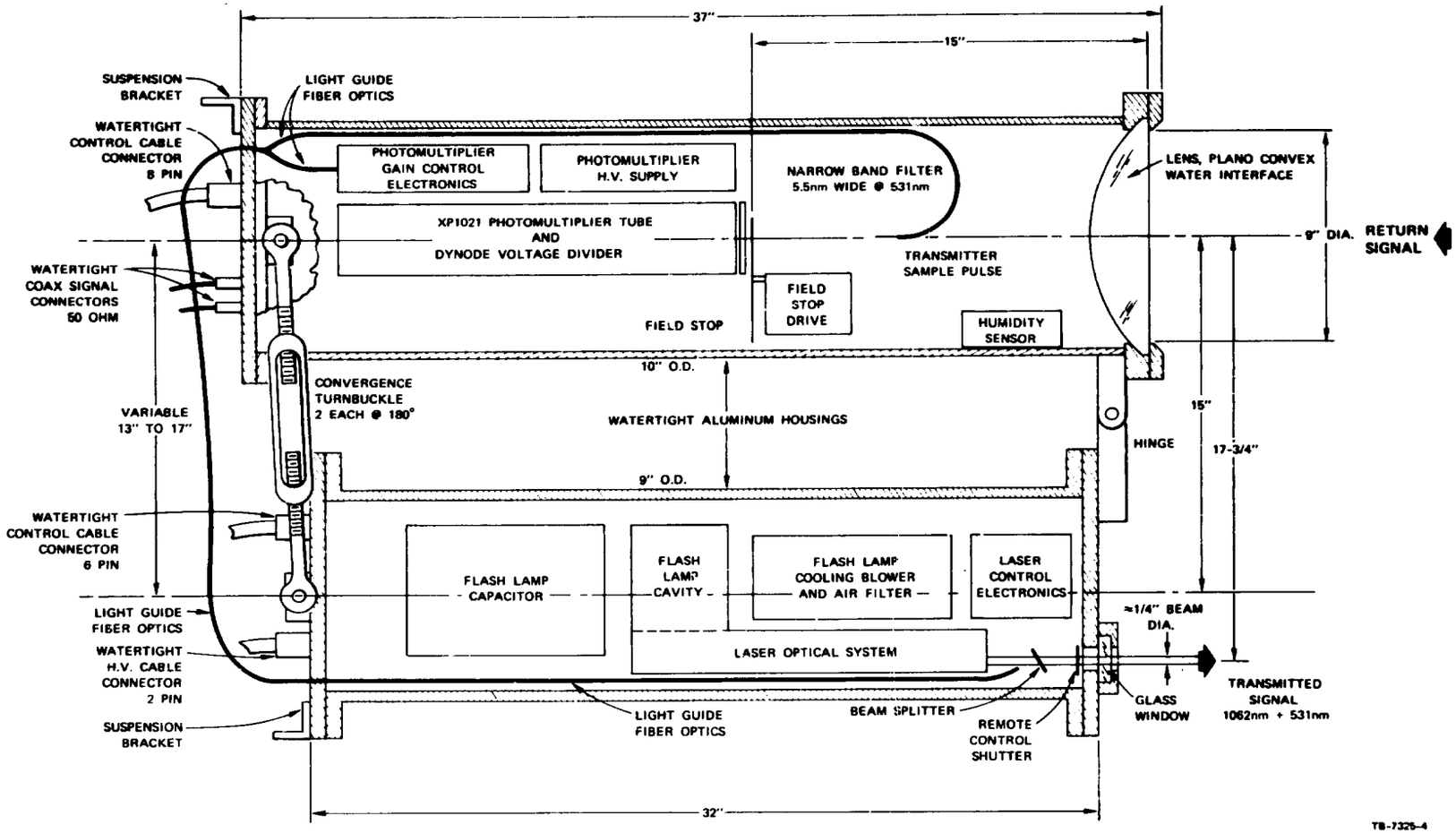

FIGURE 6 SCHEMATIC DIAGRAM OF THE UNDERWATER LIDAR SYSTEM

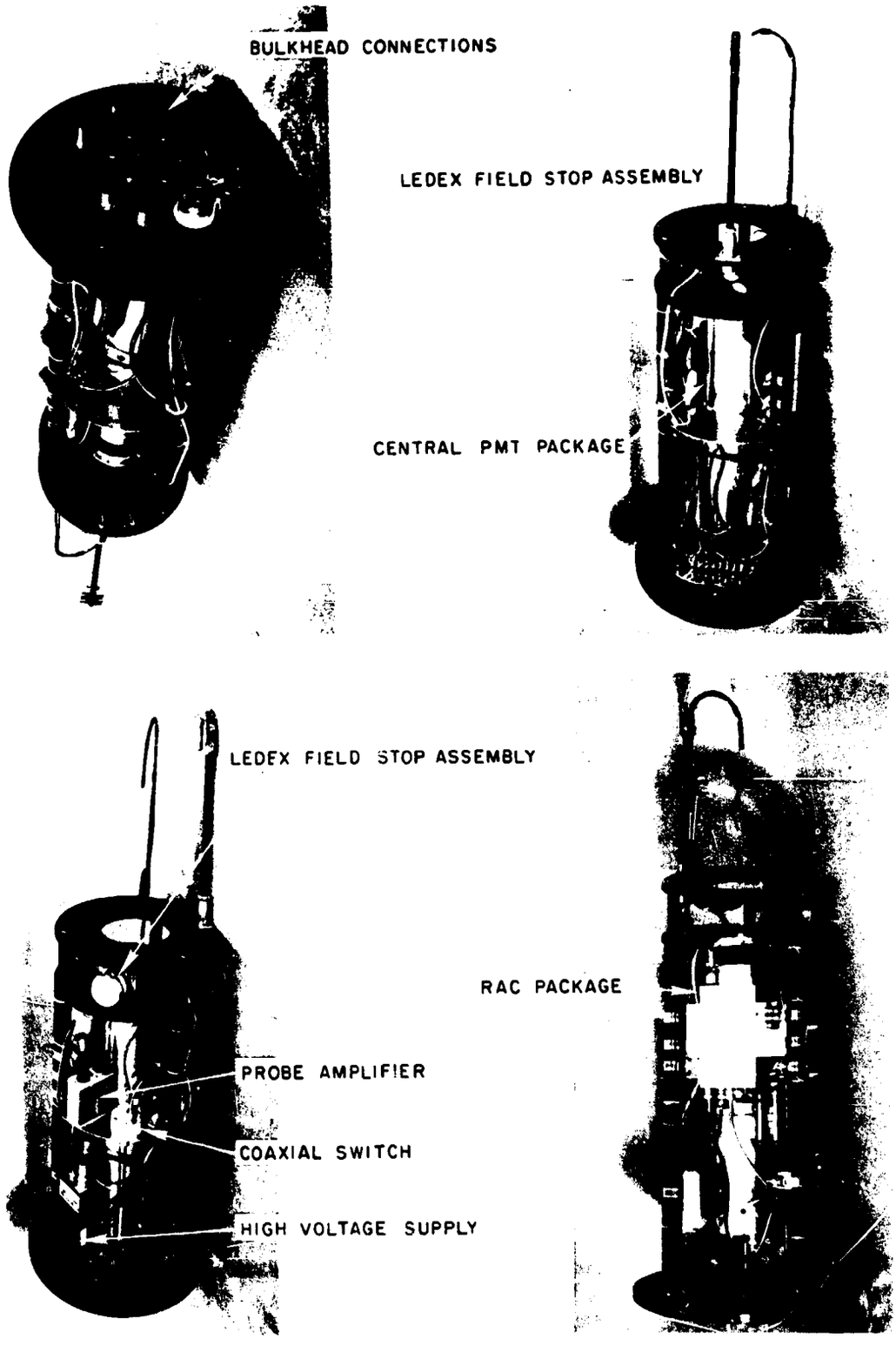

FIGURE 7 RECEIVER PACKAGE

Table III

RECEIVER FIELD OF VIEW

Position No.	Field-stop Diameter (inches)*	Field of View				Range to Beam Overlap with Optic Axes Parallel † (45.1 cm apart)											
						Start§						Complete§					
		Air		Water		Air			Water			Air			Water		
		Radians	Degrees	Radians	Degrees	Feet	Meters	ns	Feet	Meters	ns	Feet	Meters	ns	Feet	Meters	ns
0	0.0	←	Iris closed		→												
1	0.1875	0.0125	0° 43'	0.0094	0° 32'	110.4	33.7	112.2	147.2	44.9	199.5	441.7	134.6	449.1	588.8	179.5	798.2
2	0.375	0.025	1° 26'	0.0188	1° 4'	68.0	20.7	69.1	90.6	27.6	122.8	126.2	38.5	128.3	168.3	51.3	228.1
3	0.750	0.050	2° 52'	0.0375	2° 9'	38.4	11.7	39.0	51.2	15.6	69.4	52.0	15.8	52.9	69.3	21.1	93.9
4	1.500	0.100	5° 44'	0.0750	4° 18'	20.5	6.3	20.8	27.4	8.4	37.1	23.9	7.3	24.3	31.8	9.7	43.1

*Focal length = 15 inches.

†The divergence of the collimated beam due to narrow-angle forward scattering is not taken into account.

§Due to the finite size and divergence of the laser beam, the part of the beam nearest to the receiver enters its field of view at a closer range than the farthest part of the beam.

Immediately behind the field stop is located the narrow-band interference filter (5.5 nm wide, centered at 531 nm), and immediately behind the filter is a cylindrical housing containing the photomultiplier (PMT) and its voltage divider network. Since under normal biasing conditions the diameter of the useful photocathode area is slightly greater than that of the largest field stop, no additional light-focusing optics are necessary.

The rear section of the receiver housing contains a package for generating a specially-shaped 60-volt "turn on" pulse which is used to control the PMT gain during the first few hundred nanoseconds of range time. It also contains a high-voltage-power-supply module for the PMT, a video preamplifier line-driver module for the logarithmic video output, and a five-position coaxial switch to provide access to various video test points when the receiver housing is under water.

The rear bulkhead of the receiver housing contains six orifices sealed with appropriate water-tight fittings for:

(1) An eight-conductor power-input and control connector

(2) A coaxial cable connector leading from the rotor of the internal coaxial switch (This line is normally used to feed the logged video signal to the on-deck display)

(3) A coaxial cable connector for a line feeding trigger pulses and PMT unblanking waveforms to the on-deck display

(4) A control for a two-position switch for transferring between logarithmic and linear modes

(5) A control for a five-position coaxial switch

(6) A connector for a flexible fiber-optic light guide carrying a sample of the laser transmitter pulse.

Inside the receiver housing, the transmitter light sample received via the connector (Item 6, above) is divided by bifurcated fiber optics. One portion is fed to a silicon photodiode that generates a trigger pulse for the unblanking and display electronics. The other is attenuated, transported through a J-shaped light guide, and fed into the photomultiplier from a small exit aperture located just behind the center of the main collecting lens.

The receiver control unit and an oscilloscope display are located on deck at the other end of 100 feet of cable. The control unit converts 115 V, 60-Hz primary power into ±12 Vdc for all receiver electronics, and provides control for two pot-positioning motors and the field-stop stepping solenoid in the receiver. A meter is used to read out the position of the field stop.

A Tektronix Model 454 Oscilloscope (dc-150 MHz) and associated Model C40 high-speed Polaroid camera are used for the display and recording respectively.

Figure 8 is a block diagram of the entire system, and Figures 9 and 10 are photographs of the system.

C. Electrical Design Features

1. Photomultiplier Tube

The photomultiplier used in the receiver is an Amperex Type XP1021. This tube was chosen primarily because of its amplitude linearity up to large peak anode currents (up to 1 ampere), its low transit-time dispersion (less than 10^{-9} s), and its coaxial anode output connection designed for handling very fast pulses. A secondary consideration was the somewhat unique capability of electrical control of the effective photocathode diameter. Since this area modulation can be accomplished at submicrosecond rates, it was anticipated that this

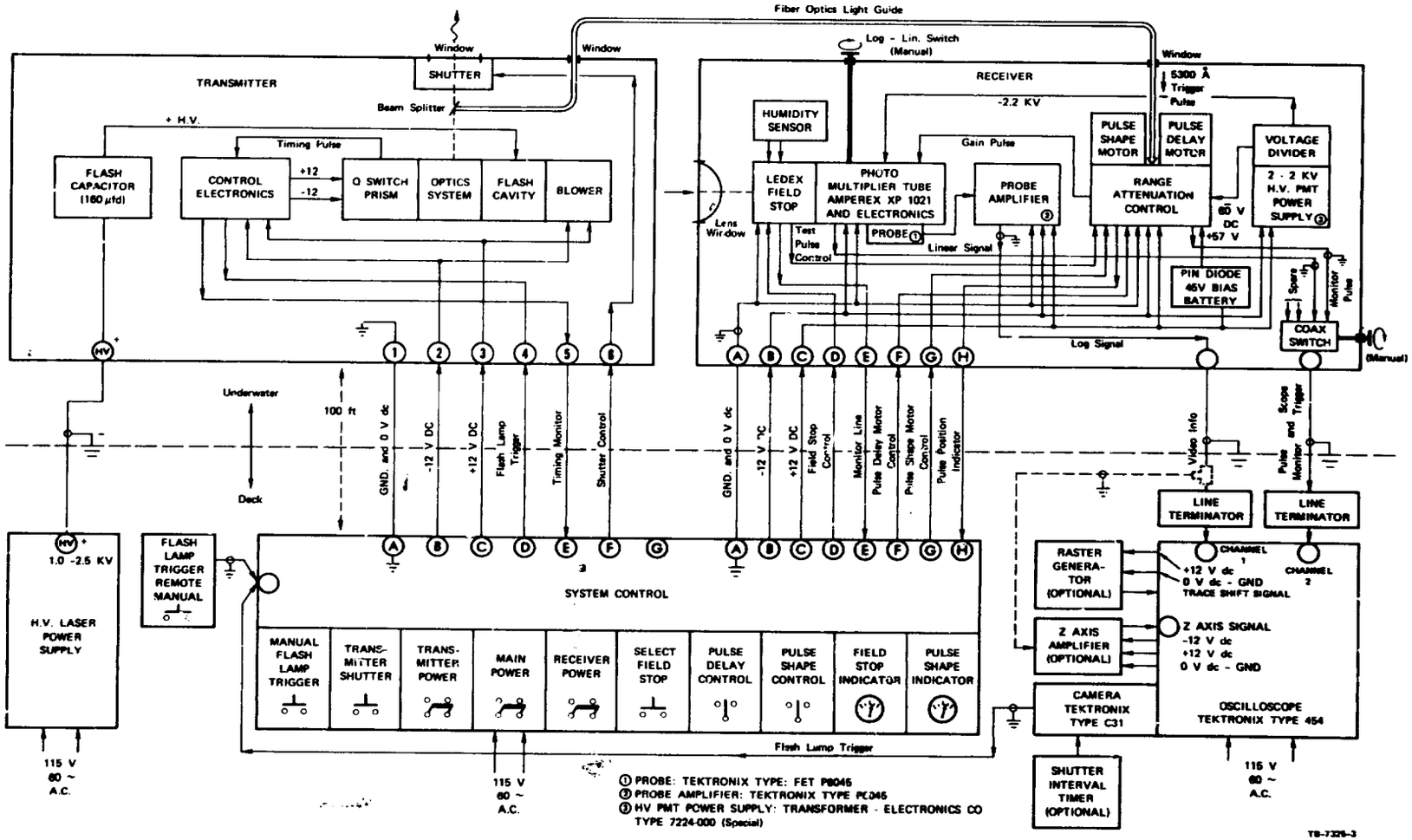

FIGURE 8 BLOCK DIAGRAM OF UNDERWATER LIDAR SYSTEM

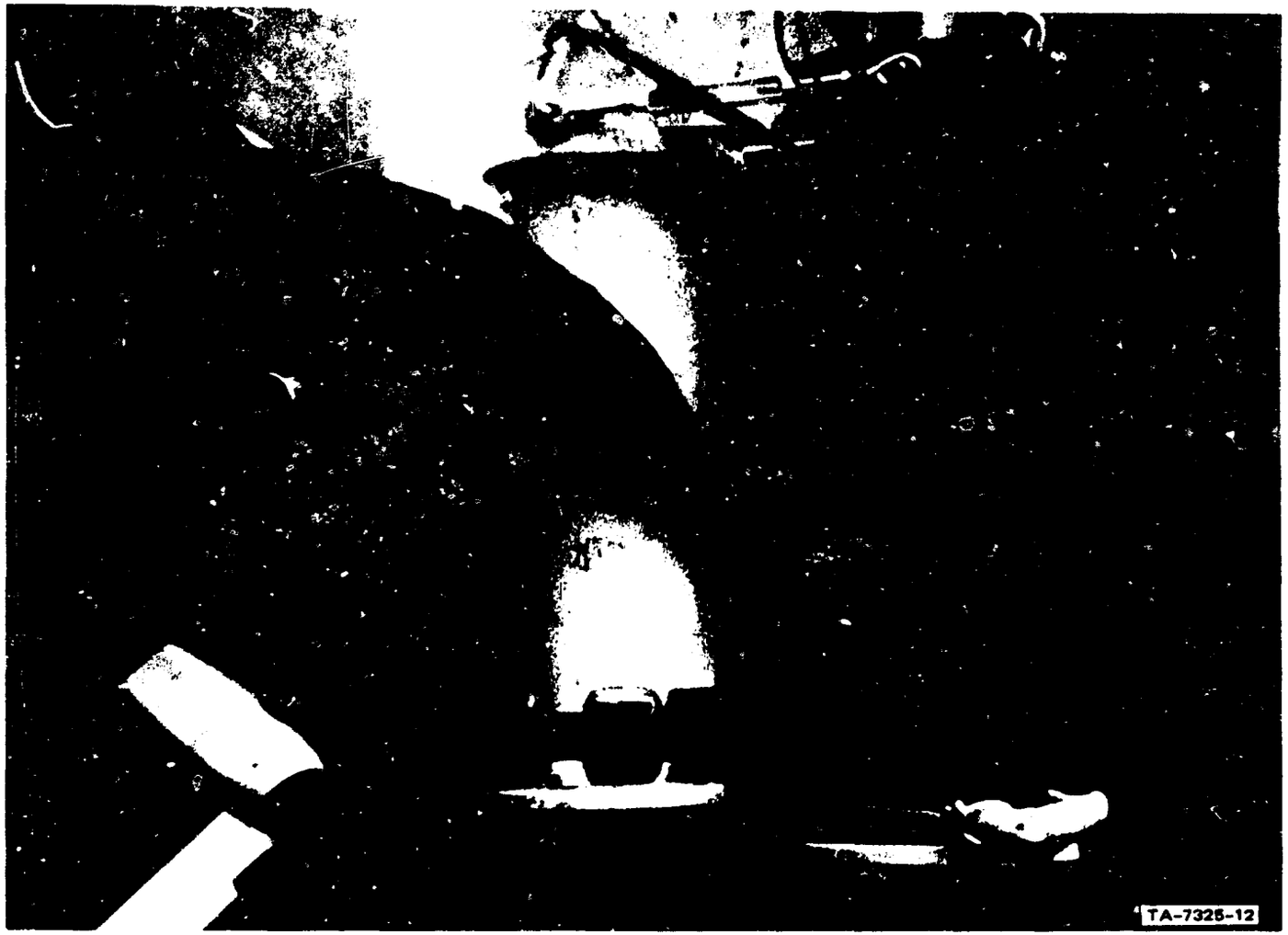

FIGURE 9 LIDAR SYSTEM IN USE UNDER WATER

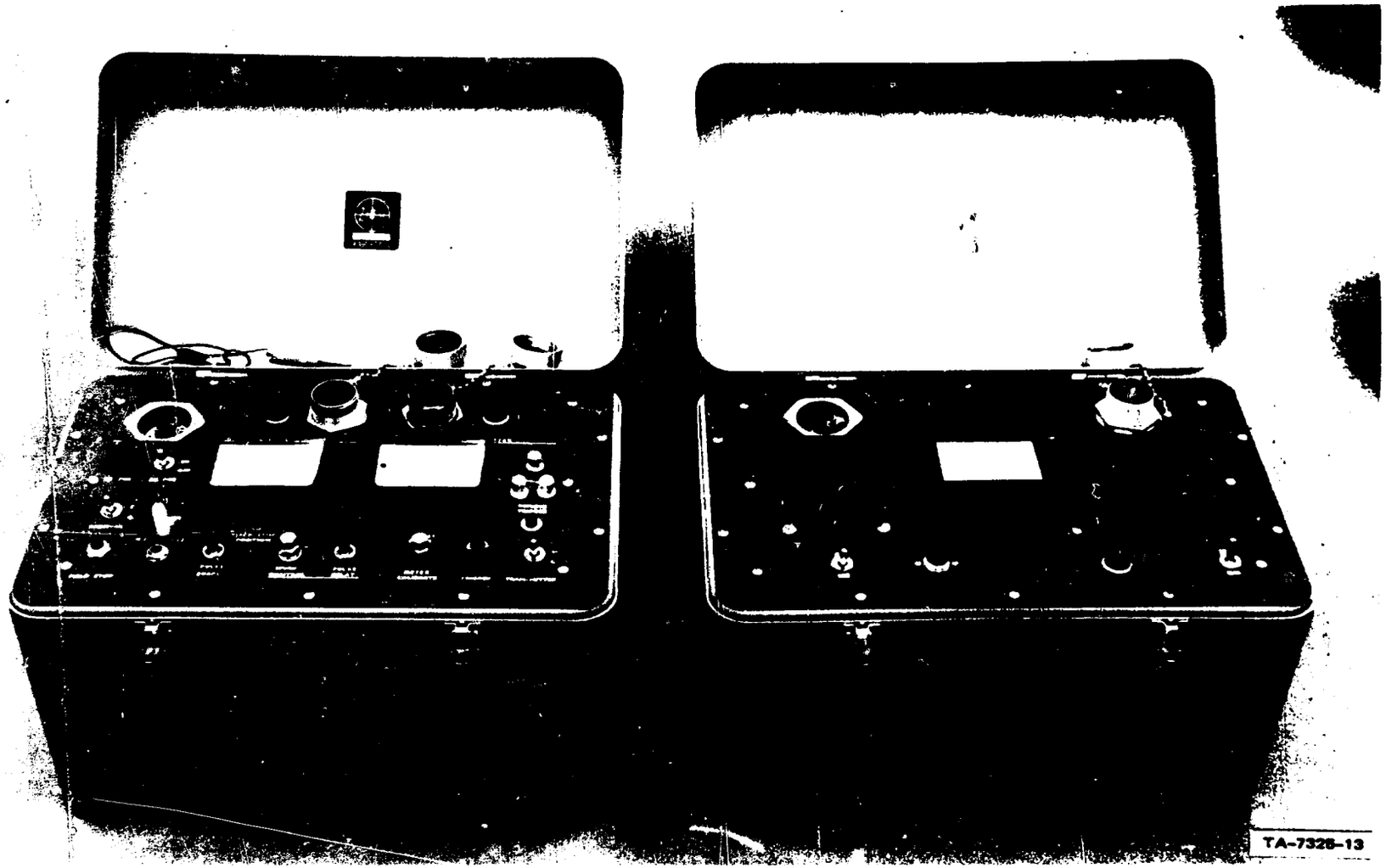

FIGURE 10 RECEIVER PACKAGE CONTROL (LEFT) AND LASER TRANSMITTER CONTROL (RIGHT)

feature might prove useful in subduing the large return from nearby backscatter. For example, by locating the photocathode in or very near the focal plane of the main lens, as it is in our receiver, the effective photocathode area then becomes the field-determining stop for the system. This makes it possible to make the field of view quite small while the transmitted pulse is near the lidar and well collimated, and to gradually widen it to accept more multiply scattered light from ranges where the return is heavily attenuated by sea water.

As it turned out, this variable-area capability has not been utilized for the following reasons:

(1) The control of effective cathode diameter for the XP1021 coaxial-output tube was found to be much less complete than that obtained in the parent, but non-coaxial, tube type, the Amperex 56AVP. A 4:1 diameter change was all that could be achieved, and the effective spot became both elliptical and fuzzy-edged at the smaller sizes.

(2) It was found that a much greater range of dynamic-gain control could be achieved with a moderate amplitude-control pulse, by modulating the potential of alternate dynode elements along the multiplier chain.

In view of the seriousness of the afterpulsing problems later experienced at very high light levels, and the knowledge that the problem originates at or very near the front end of the tube, it is possible that more careful attention should now be directed to use of the G1 (area-controlling) electrode. However, a preliminary investigation revealed little or no effect of G1 in reducing afterpulsing.

The voltage-dividing circuit for the photomultiplier tube is shown schematically in Figure 11 and photographically in Figure 12. The high voltage to the photomultiplier chain is supplied by a 10-watt, fully encapsulated, regulated power supply from Transformer-Electronics Company, obtained with a special 21-to-27-Vdc input. As implied above, the receiver, as implemented, achieves range-attenuation control (RAC) through dynode modulation. If the potential of one dynode is changed while holding the potential of the two adjacent dynodes constant, the gain of one of the stages will increase slightly while the gain of the other stage will decrease severely. The overall effect is a net gain decrease for dynode potentials very far either side of optimum. Tests showed that for our tube a slightly more linear control characteristic resulted from modulation on the positive side of the maximum. For each pair of stages so controlled, approximately 20 dB (100X) of gain reduction can be realized with a control-voltage swing of less than 100 volts.

Thus, dynodes D2, D4, D6, and D8 (Figure 11) are provided with individual calibrated pots for adjusting their static potentials. For the pots of D4, D6, and D8, full clockwise provides the optimum (high-gain) potential--i.e., approximately midway between the two adjacent dynode potentials. Full counterclockwise provides zero potential difference between the controlled dynode and the next higher dynode, and results in minimum gain. The control for D2 was arranged to give a permissible potential anywhere between D1 and D3--i.e., maximum gain occurs near midrange.

Normally, the "resting" gain of each of the controlled stages is reduced about 10 to 15 dB below maximum via the static bias controls. Then a negative-going 60-volt pulse having a relatively slowly rising leading edge is applied via capacitive coupling in parallel to all of the four controlled dynodes. This results in a gradual increase of the

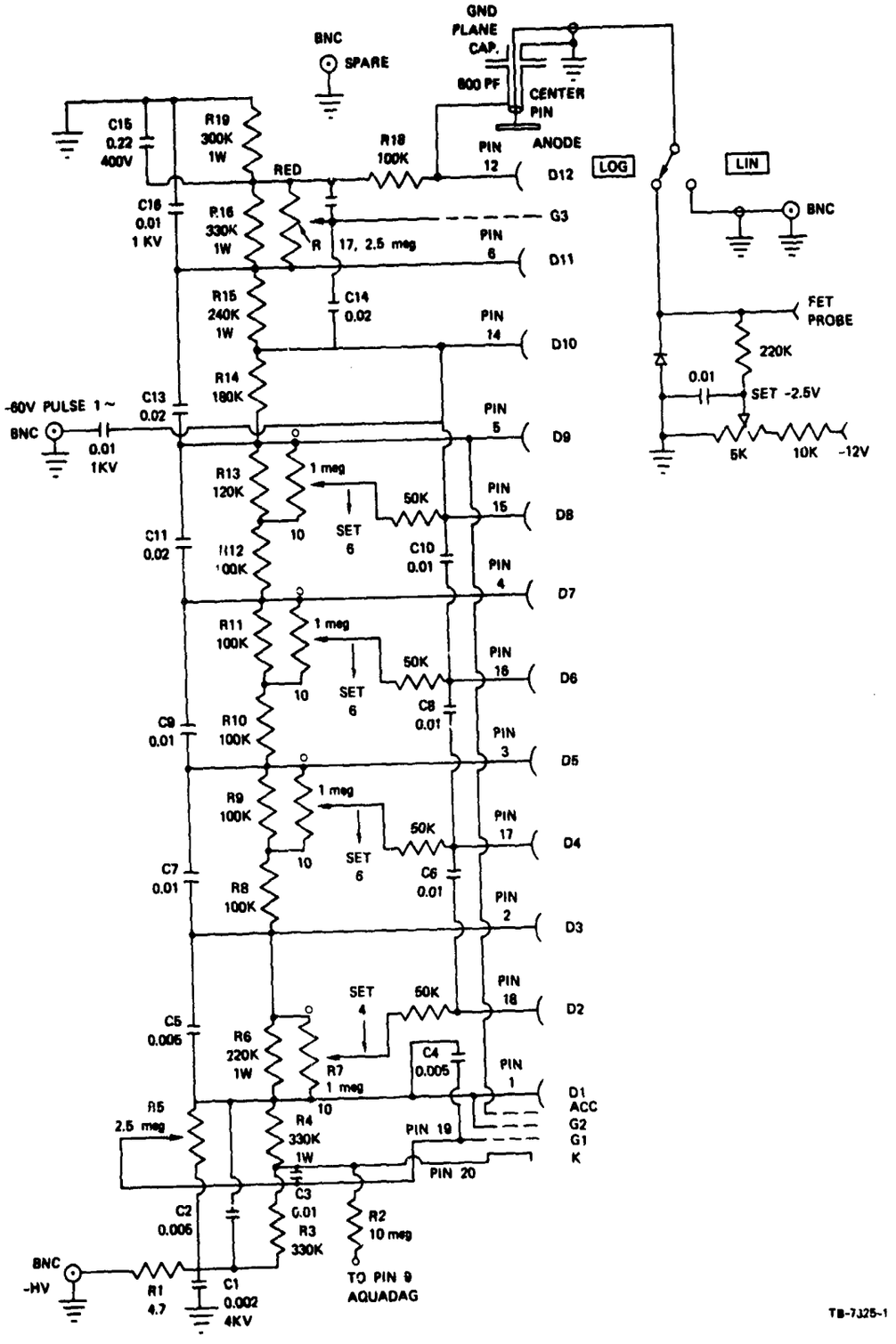

FIGURE 11 PHOTOMULTIPLIER TUBE WIRING DIAGRAM

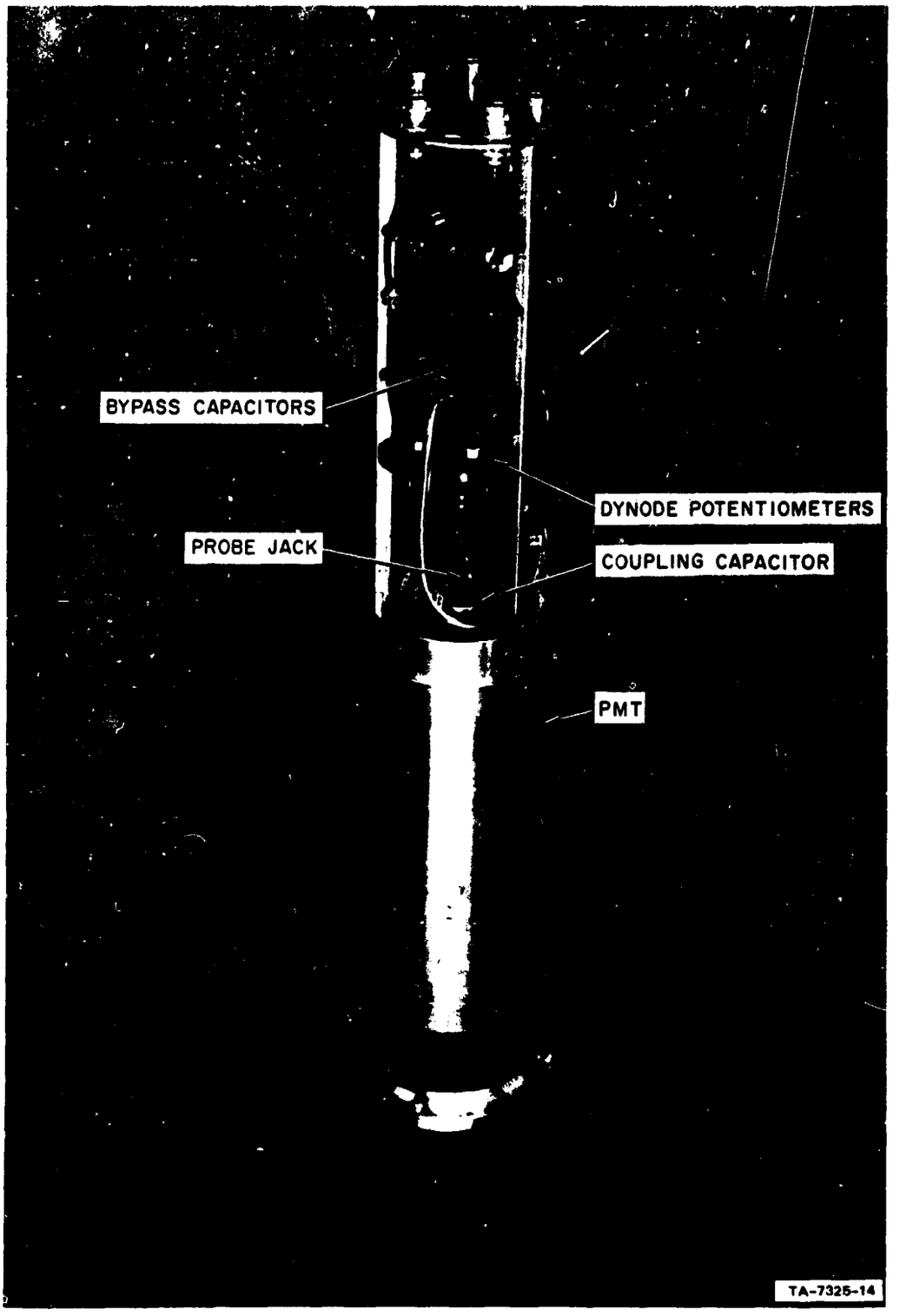

FIGURE 12 PHOTOMULTIPLIER TUBE PACKAGE

overall multiplier gain to or near its maximum value. The maximum gain condition is maintained for approximately one microsecond. Then the "turn on" pulse decays, and the gain returns to its resting value.

2. Range-Attenuation Control

The details of the range-attenuation control based on the above principles is shown in Figure 13. The "turn on" waveform is generated first as a rectangular one-microsecond pulse, delayed from the trigger pulse by an adjustable amount determined by a one-shot multivibrator which in turn is controlled by a motor-driven pot. The leading edge of the pulse is then rounded to an exponential curve via an RC coupling network whose time constant can be adjusted remotely via another motor-driven potentiometer.

To facilitate making these adjustments, a sample of the shaped "turn on" pulse is additively mixed with the trigger pulse from the silicon photodiode before transmission up the trigger line to the deck. There the combination can be viewed or photographed on the oscilloscope while adjustments are made with the receiver control box.

As a further aid in setting up, a test oscillator in the receiver can be activated from the on-deck control box to generate synthetic trigger pulses at a 1-kHz rate, high enough to provide a repetitive display sufficiently bright to observe without a viewing hood. These various waveforms are shown in Figures 14 and 15.

3. Logarithmic Amplifier

The video amplifier with the logarithmic response makes use of the fact that the voltage developed across a forward-biased semiconductor junction diode is closely proportional to the logarithm of the current through the diode.

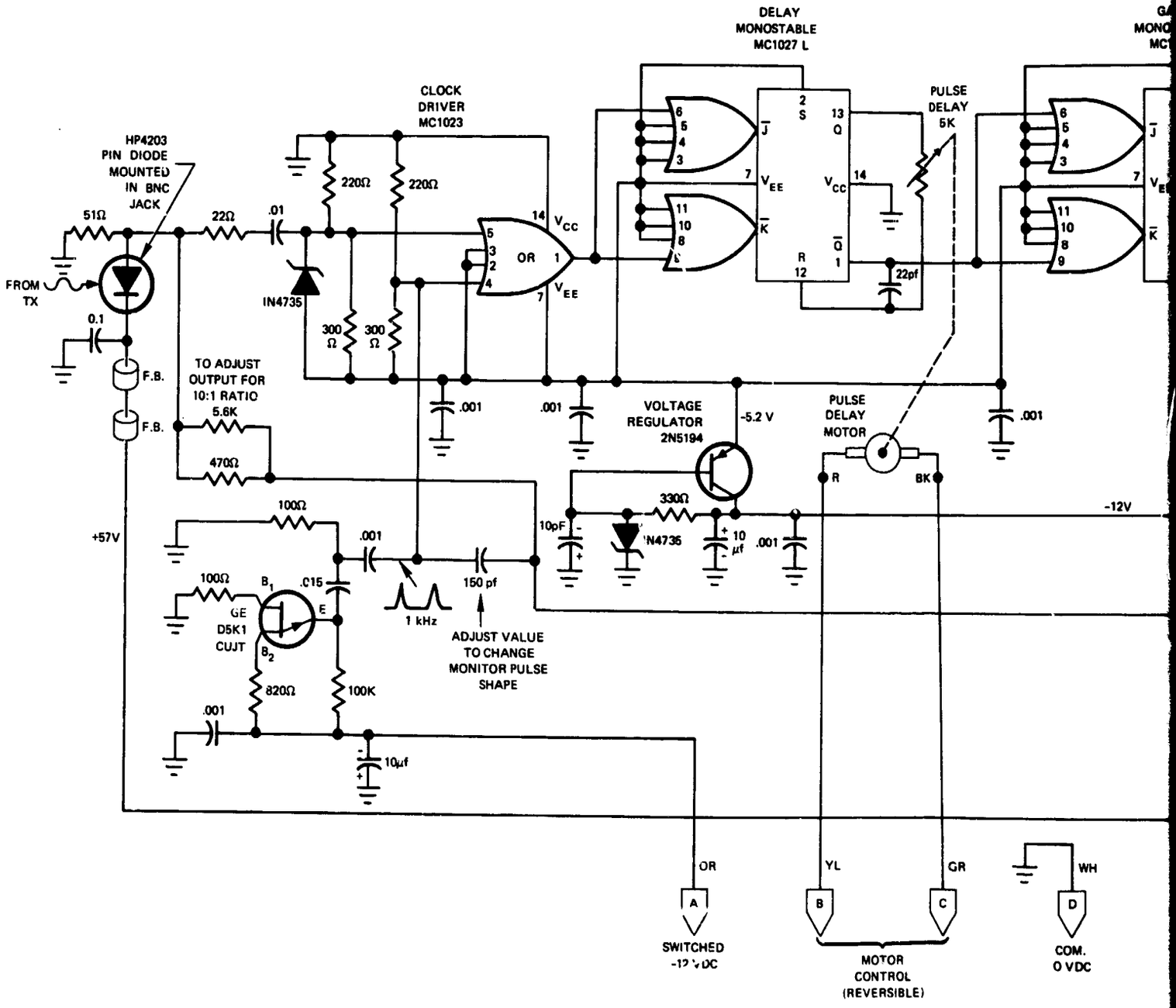
DELAY
MONOSTABLE
MC1027 L
CLOCK
DRIVER
MC1023
HP4203
PIN DIODE
MOUNTED
IN BNC
JACK
51Ω
22Ω
.01
220Ω
220Ω
FROM
TX
0.1
IN4735
300
Ω
300
Ω
OR
V_{CC}
V_{EE}
PULSE
DELAY
5K
22pf
F.B.
F.B.
TO ADJUST
OUTPUT FOR
10:1 RATIO
5.6K
470Ω
.001
.001
.001
VOLTAGE
REGULATOR
2N5194
-5.2 V
PULSE
DELAY
MOTOR
R
BK
-12V
330Ω
10pF
IN4735
10
μf
.001
+57V
100Ω
.001
100Ω
B_1
.C15
E
GE
D5K1
CUJT
B_2
820Ω
100K
.001
10μf
150 pf
1 kHz
ADJUST VALUE
TO CHANGE
MONITOR PULSE
SHAPE
OR
YL
GR
WH
A
B
C
D
SWITCHED
-12 VDC
MOTOR
CONTROL
(REVERSIBLE)
COM.
0 VDC

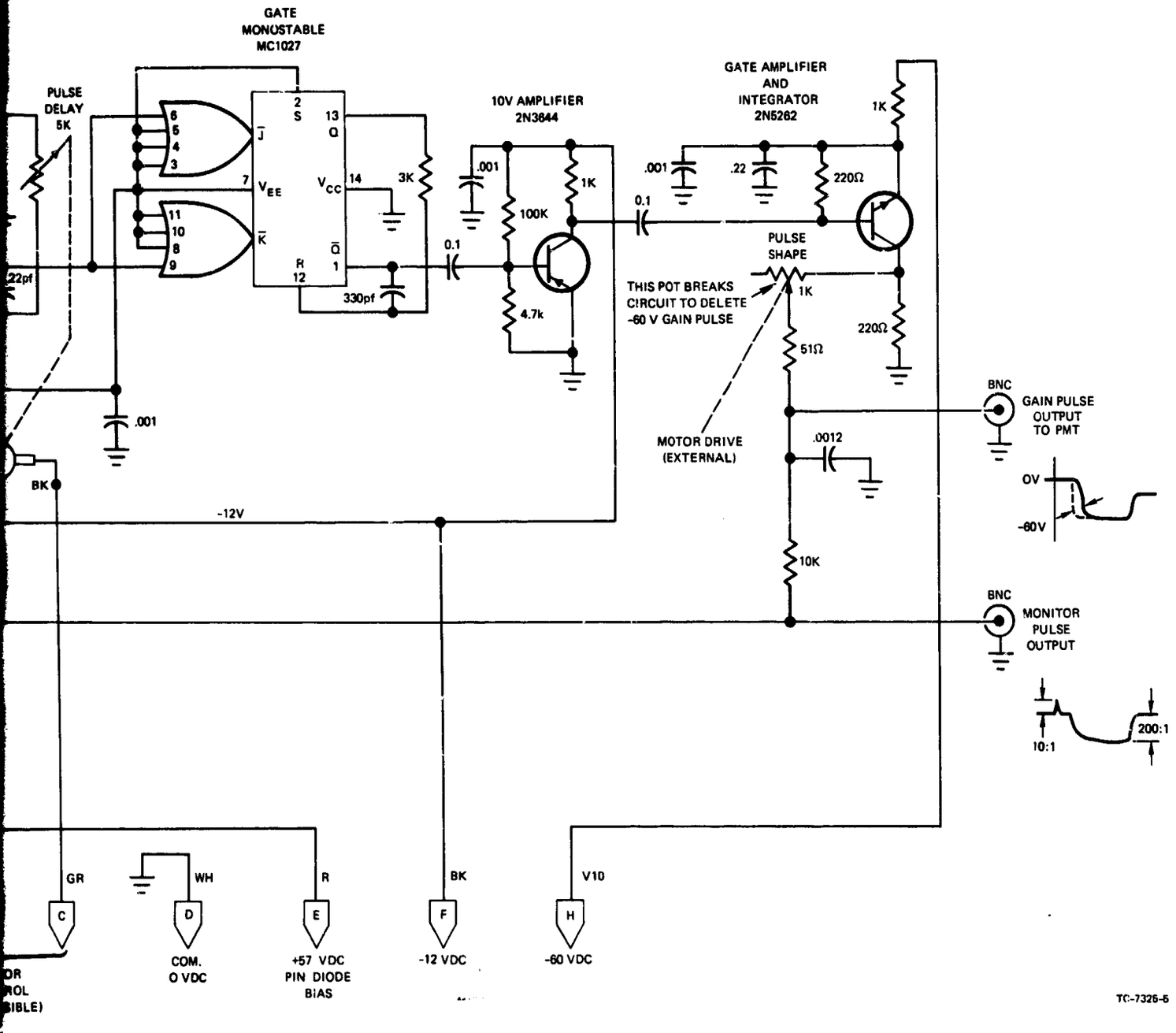

FIGURE 13 SCHEMATIC DIAGRAM OF RANGE ATTENUATION CONTROL

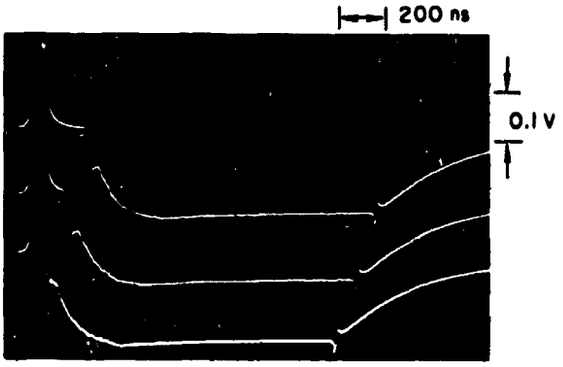

FIGURE 14 "TURN-ON" PULSE AT VARIOUS DELAYS FROM THE TRIGGERING PULSE

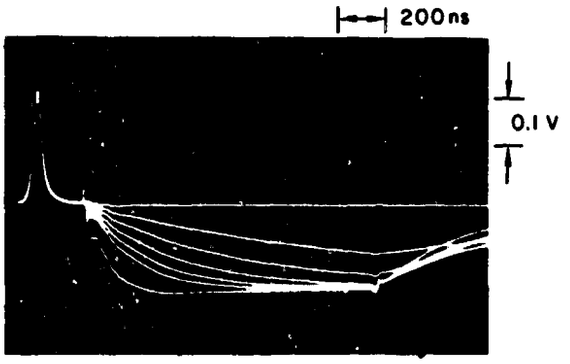

TA-7325-15

FIGURE 15 "TURN-ON" PULSE WITH VARYING RISE TIMES

Theoretical analysis of the behavior of a forward-biased semiconductor PN junction leads to Eq. (1), which is found in virtually every semiconductor text. Gray et al.[5] give a particularly lucid treatment:

$$I = \left[\exp\left(V/V_T\right) - 1\right] I_s \qquad (1)$$

where

I is the dc current through the diode

V is the dc voltage across the diode

V_T, sometimes called contact potential or the junction voltage, is related to the absolute temperature T, Boltzmann's constant k, and the electronic charge e:

$$V_T = kT/e \qquad (2)$$

[V_T has the dimensions of volts and at room temperature has a value of V_T (300° K) = 26 mV.]

I_s is the saturation current--the component of current through the reverse-biased diode that is not attributable to leakage effects and is nearly independent of reverse voltage. It is a function of the diode material and the degree of doping, and is extremely sensitive to temperature. For germanium junction diodes, I_s is in the region of 10^{-4} to 10^{-5} amp. For silicon, it can be 3 to 12 orders of magnitude less (10^{-8} to 10^{-9} amp are typical values).

Rearrangement of Eq. (1) gives

$$V/V_T = \ell n\ (I/I_s + 1) \qquad . \qquad (3)$$

For all except extremely small values of I, the 1 can be ignored and the relation is seen to be

$$V = V_T\ \ell n\ I - V_T\ \ell n\ I_s \qquad (4)$$

or

$$V = 2.303\ V_T \log I - 2.303\ V_T \log I_s \quad . \qquad (5)$$

Equation (5) would plot as a straight line on semilog paper; it would have a slope of 2.303 V_T, or 60 mV/decade of current at room temperature, and the line would intersect the current axis at I_s when V = 0.

Published values of Stuart[6,7] and Slice[8] and our own measurements show that actual diode junctions follow the general logarithmic law quite closely, but that usually the slope is somewhat greater than predicted by Eq. (5).

Figure 16 gives the results of dc measurements made at two temperatures on an FDM 6000 silicon junction diode, which is a type that we have found particularly useful for high-frequency logging because its logarithmic characteristic extends further into the high-current (low-impedance) region than most. The curves are seen to be linear to better than 1 dB over more than four decades of input current. The slope at room temperature is about 120 mV/decade, or twice that predicted by Eq. (5). The slope of the characteristic also indicates the small-signal, low-frequency dynamic resistance of the diode for different values of dc bias current, I. Because of the characteristic, these resistances will be inversely proportional to I. For the room-temperature curve of Figure 16, the equivalent resistance values are about 4 ohms at I = 10 mA, 40 ohms at I = 1 mA, 400 ohms at Ia = 0.1 mA, etc., down to 40,000 ohms at 1 μA. The curves were not extended to lower values of current (higher dynamic resistances) because the unavoidable circuit capacitances will not permit attaining the required high-frequency response at impedance levels greater than a few thousand ohms.

At high current levels, the curves depart quite noticeably from the logarithmic characteristic. At 0.5 amp, for example, the slope has

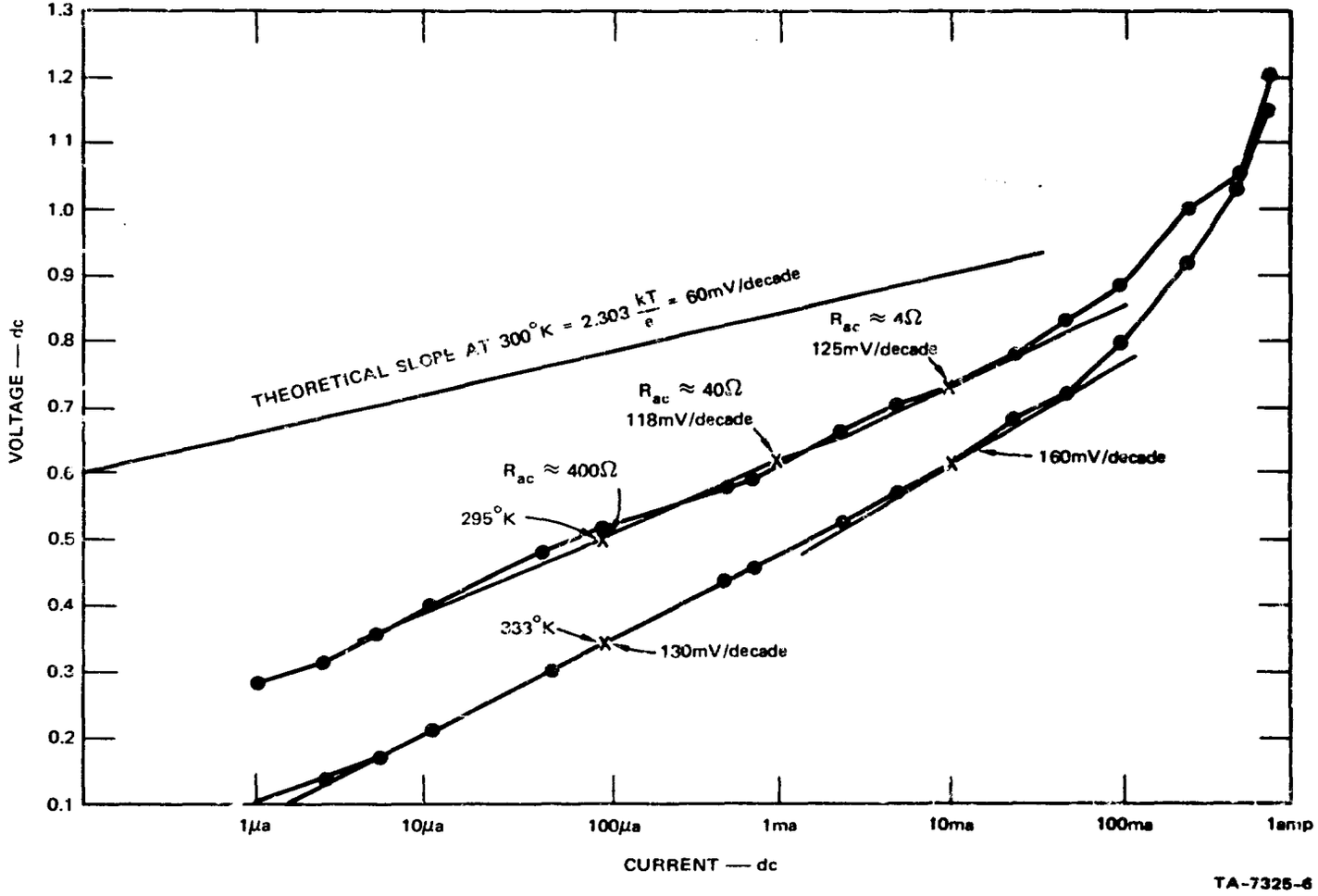

FIGURE 16 MEASURED dc CHARACTERI[S]TICS OF FCM 6000 Si JUNCTION DIODE

increased to about 420 mV/decade, which at that current level corresponds to a dynamic resistance of 0.42 ohm. The dc resistance at the same point is down to 2 ohms. This is down in the region where the bulk resistance of the silicon and the ohmic resistance of the connections become predominant; above a few hundred milliamperes, the diode behaves more and more like a simple resistor.

Thus, the useful range of the FDM 6000 diode for video-frequency logging applications covers four decades of current, from 10^{-1} A to 10^{-5} A. Fortunately, the upper end of this range is very conveniently matched to the maximum output currents that can be produced with good linearity by the XP1021 multiplier phototubes. Thus, the maximum available dynamic range of the diode can be utilized without further current gain.

As mentioned above, at low anode current levels (say, at 0.01 mA), and with a practical minimum circuit capacitance (say, 10 pF), the discharge time constant is on the order of 40 ns and thus will become the limiting factor in determining range resolution for signal levels in this level or below. For anode currents above approximately 0.1 mA, the logger does not appear to degrade the system pulse response appreciably.

The voltage across the logarithmic diode is probed with a Tektronix P6045 probe which is a high-gain-bandwidth low-capacitance 1X probe. The probe has a high input impedance achieved by means of a field-effect transistor built into the probe tip, followed by amplifier and dc offset circuits. The dynamic range of the probe output is from +500 mV to -500 mV. The logarithmic diode dc biasing circuit leaves the probe at -0.4 volts. The dc offset is used to put the probe output at this time at +0.5 volts, enabling the probe to respond over the range -0.4 to -1.4 volts, covering the dynamic range of the logarithmic diode adequately.

4. Video Output Coupling

When attempting to preserve the shape of analog waveforms that change drastically in tens of nanoseconds, the physical layout of components and ground-return paths always become very critical. For our application, where it was desirable to provide an option of a logarithmic amplitude response for the display, the problem was especially annoying since an overshoot or ring of a few percent, which would hardly be noticed on a linear display, stands out very prominently on a logarithmic display because of the increased emphasis given to low-level signal components.

A useful source of short test pulses for checking the PMT and associated video circuitry is the cathode thermal emission component of the PMT dark current. For the multiplier gains obtainable with the XP1021 tube ($\mu = 10^8$), a single electron leaving the photocathode will result in an anode current pulse, $I = \mu e/t$, of several milliamperes peak, and several nanoseconds width. This amplitude is comparable to the mid-range of typical lidar return levels, and the rise and fall times are comparable to the best that might be expected from the laser pulse.

Even with the unique coaxial output connector provided on the XP1021 photomultiplier tube, considerable trouble was experienced in achieving what was judged to be an acceptable response to such very short pulses. One problem is that in order to minimize lead inductance within the tube, the outer conductor of the output coaxial connector is connected directly to the last dynode, thus adding the requirement that approximately 200 volts of dc potential must somehow be blocked from the millivolt-level video output circuit. The configuration finally adopted is shown schematically in Figure 11 and photographically in Figure 17. A key element is the flat, two-disc by-pass capacitor. In an early version of the logarithmic amplifier, the grounded disc of the

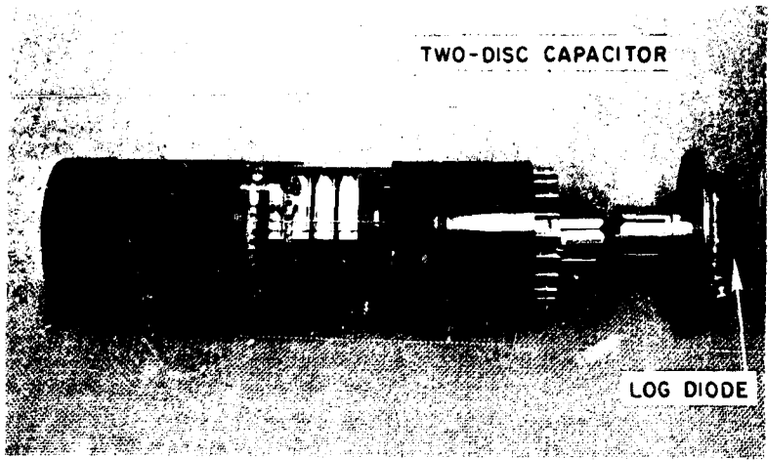

(a)

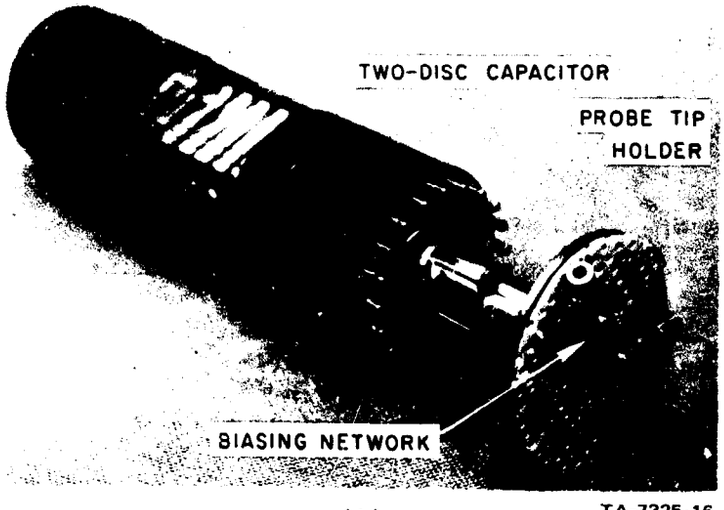

(b)

TA-7325-16

FIGURE 17 DETAILS OF PHOTOMULTIPLIER OUTPUT COUPLING

capacitor served as the "chassis" for the complete amplifier. When this amplifier was later replaced by a commercially available, probe-mounted preamplifier, the capacitor structure was retained. The General Radio coaxial connector supplied with the PMT was pared down to reduce its shunt capacitance. The logarithmic diode along with a dc biasing network to set its minimum current to 10 microamperes, a low-capacitance log-linear transfer switch, and a holder for the probe tip were mounted on the grounded disc of the capacitor to minimize lead inductance.

IV PERFORMANCE OF THE UNDERWATER LIDAR SYSTEM

Preliminary tests of the lidar system were conducted under laboratory conditions in the atmosphere using various target systems. The lidar system performed entirely as expected at this stage.

The performance of the lidar system was then tested in ocean water on three occasions--June 25, June 30, and August 22, 1969. All three tests were made in the Pacific Ocean, a few miles off the Monterey Peninsula in Northern California. They were performed on board a U.S. Naval Postgraduate School hydrographic research vessel. The use of this 63-ft converted air-sea rescue boat was arranged through the courtesy of Dr. Stevens P. Tucker, Jr., of that school.

In all the trips, the procedure was to load the gear in the morning, cast off about 9 a.m., and arrive at some point with relatively clear water at about 10:30 a.m. The tests began at about 11:00 a.m. and continued till around 2:00 p.m., moving to different locations if necessary, and arriving back at the docks at about 4 p.m.

On board the vessel there was an enclosed area near the stern in which the control and display packages were located, along with operating personnel. A motorized winch and an A-frame were available to maneuver the lidar assembly and lower it over the side into the water. Lead-weight belts were used to sink the assembly in the water. A spar buoy attached with a length of line controlled the depth to which the system was submerged, with the transmitter aimed downward. This arrangement decoupled the system from the surge of the vessel. A photograph of the system under water appears as Figure 9.

The first test, on June 25, 1969 was helpful in gaining experience in handling the system and establishing operating procedures. After an hour of testing, the transmitter stopped lasing. A thermal effect was suspected as the laser started functioning when the system was pulled out of the water and allowed to warm up. The temperature of the ocean at this location was about 50°F. It was found later in the laboratory that the temperature-sensitive component was a trigger tube. When the tube was replaced the system performed well at all temperatures tested.

The second trip was made on June 30, 1969. The system performed well as a package for over three hours. Samples of the data obtained are shown in Figure 18. In these pictures the upper trace is the photomultiplier output signal modified by the logarithmic amplifier.

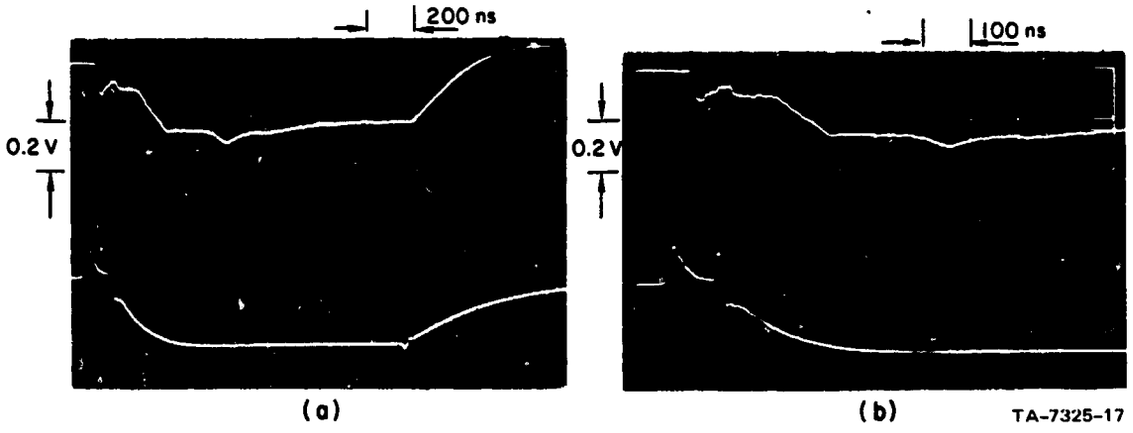

FIGURE 18 LIDAR RETURNS UNDER WATER OFF MONTEREY, 30 JUNE 1969.
Receiver Field Stop 4.

The lower trace shows the monitor signal consisting of the PIN diode output and the amplification "turn on" profile. The sharp transient corresponds to the beginning of the amplification "turn on." It was found that the gross features of the signal return displayed by the scope were invariant over a long period of time and at three different locations. At first the peak at about 600 ns after the monitor pulse was thought to be a reflection from the bottom at approximately 200 feet.

When identical returns were obtained in two other locations in very deep water (600 fathoms), the displayed signal was suspected to be the result of factors internal to the receiver package.

On experimentation in the laboratory, it was found that the sample of the laser pulse arriving at the photomultiplier through the J-shaped light guide supplied a high-intensity light pulse that subsequently resulted in the photomultiplier producing a signal, shown in Figure 19(a), that was identical to the lidar returns obtained under water.

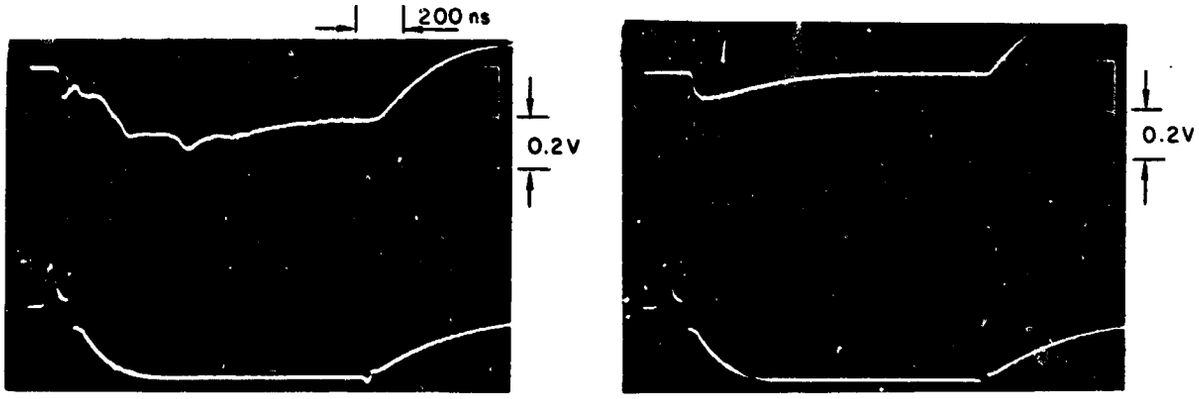

(a) INTERNAL FIBER OPTICS SUPPLYING SAMPLE OF LASER PULSE. Compare with Figure 18(a).

(b) FIBER OPTICS BLOCKED

TA-7325-18

FIGURE 19 PMT RESPONSES WITH RECEIVER LENS COVERED. Receiver Field Stop 4.

When the sample pulse appears at the cathode the amplification of the PMT is "turned down." Thus only a small anode-current pulse is produced with a delay on the order of 50 ns after the monitor pulse. This delay is due to the transit time of the fiber optics and the "turned down" photomultiplier. However, the high intensity of the sample light pulse overloads the tube and produces a lingering cathode signal higher than the usual background current. This signal grows as the tube amplification is "turned up." This overload behavior was eliminated by blocking the laser light sample, as shown in Figure 19(b), where the anode signal starts when the amplification is being turned up, more than 100 ns after the monitor pulse. (This signal is due to electrical crosstalk from the -60 V "turn on" pulse, and is not due to light input at the cathode.)

Particularly characteristic of the behavior under overload is the afterpulse at about 600 ns after the initial monitor pulse. Of course, it should be noted that the logarithmic amplifier emphasizes this low-level peak. Considerable effort was spent in tracking down and attempting to suppress or eliminate the afterpulse. It has been definitely established by probing the dynode currents along the chain, that this afterpulse is due to problems at the photocathode end of the PMT. It is surmised that the lingering signal and the afterpulse derive from a space charge formed in the cathode region of the tube when the cathode is severely overloaded. The multiplication behavior is highly irregular when the input pulse exceeds about 10^{-10} joule in a pulse of 10-ns duration (10^{-2} watts).

It appears that except for the afterpulse the tube responds almost normally even during the 600 ns preceding the appearance of the afterpulse. In fact, it has been found that two overloading pulses within 70 ns of each other will produce similar responses, with two afterpulses

appearing in the proper time relationship. Further, when a real signal of sufficient strength is present, the afterpulse can be suppressed. This can be seen in Figure 20, which shows the system output while looking at daylight sky, with and without the overloading caused by the laser sample. The responses after the tube gain has been turned up are seen to be similar, even though the initial behaviors are different.

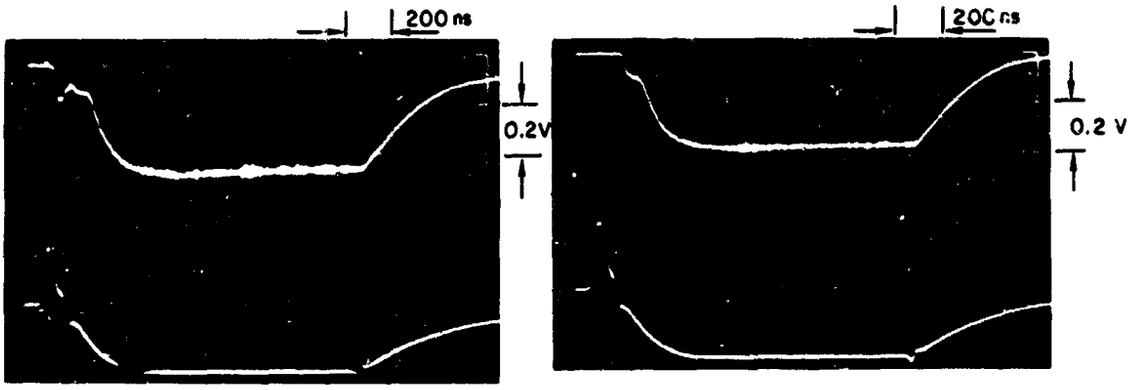

FIGURE 20 LIDAR RETURNS IN DAYLIGHT SKY WITH LASER OUTPUT BLOCKED. Receiver Field Stop 4.

Hence the problems on the second field trip were attributed entirely to the high-intensity laser sample overloading the tube and overpowering any real signal return from the water. Further experimentation was directed at reducing the electrical crosstalk that threatened to cloud the analysis of the returns at short ranges. While it was not possible to eliminate all spurious signals simply, considerable reduction was achieved. Further improvement would be possible with more elaborate shielding.

The third field trip was delayed by difficulties with the laser transmitter and was eventually made on August 22, 1969. A relatively clear stretch of water was reached for the tests. From Secchi-disk measurements, the diffuse attenuation coefficient k was estimated to be in the range 0.1 to 0.2 m^{-1}. In order to get discrete high-level

returns under water for range and intensity calibration, arrangements were made to have a white target under water. Scuba divers attempted to aim the system at the target. The complete system was used under water over a period of several hours and performed reliably.

The underwater signal returns under various system conditions are shown in Figures 21 through 25. It can be observed in Figure 21(a) that the crosstalk is substantially reduced from previous levels. The underwater upward-irradiance background was measured by operating the system with a mechanical shutter preventing the laser beam from entering the water. This background is seen in Figure 21(b) to be at a reasonable level below signal levels. This indicates, in addition, that difficulties of the second trip have been removed and that the receiver is responding to legitimate external signals only. From this and other measurements, the PMT amplification during the "on" time is estimated to be about 10^4.

The effect of changes in the field of view on the return signal is evident in Figures 22 and 23. Consecutive shots made at intervals of 10 to 15 seconds are shown in Figures 23 and 25. The returns from the underwater target are seen in Figures 23(d), (e), and (f) at a range of about 200 ns or about 70 feet, as sharp spikes above the almost constant pattern of the regular return.

However, it is recognized that the overloading of the photomultiplier is still present and evident in the afterpulse that appears at about 600 ns after the monitor pulse. It is seen in all the lidar returns shown in these figures. The clues as to the origin of the overloading signals are found in Figure 24. These returns were obtained with a delay of 200 ns between the monitor pulse and the "turn on" pulse to the PMT dynodes, whereas the previous returns were obtained with a delay of less than 20 ns. (There is a delay of about 6 ns due to the

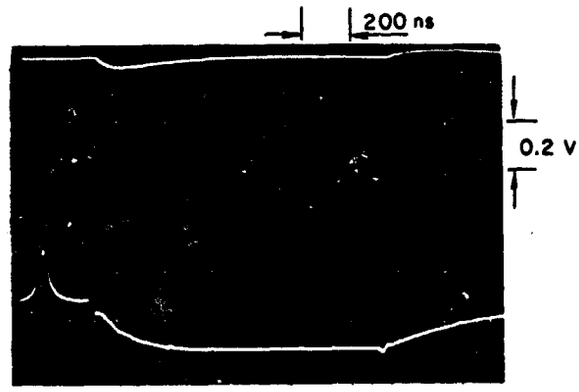

(a) PMT SIGNAL WITH RECEIVER CLOSED AND 200-ns AMPLIFICATION DELAY

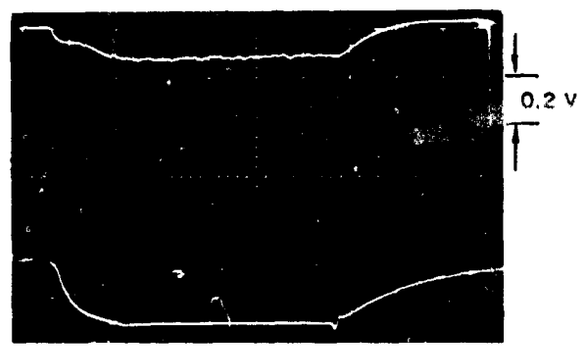

(b) UPWARD IRRADIANCE SIGNAL WITH RECEIVER FIELD STOP 3 AND LESS THAN 20-ns AMPLIFICATION DELAY

TA-7325-20

FIGURE 21 SYSTEM PERFORMANCE TESTS

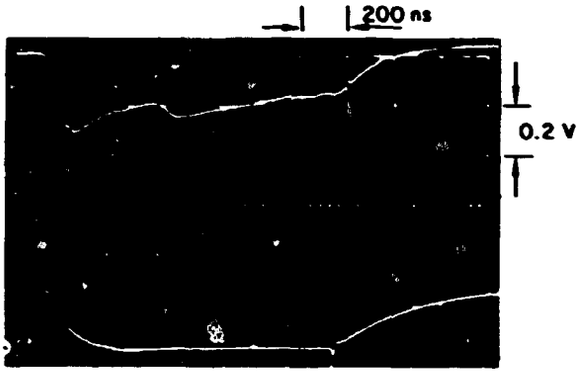

(a) RECEIVER FIELD STOP 4

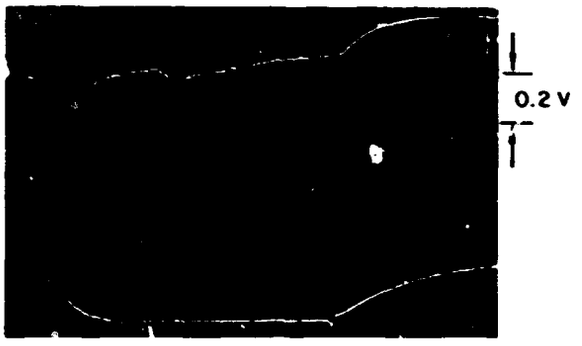

(b) RECEIVER FIELD STOP 3

TA-7325-21

FIGURE 22 LIDAR RETURNS UNDER WATER OFF MONTEREY. 22 AUGUST 1969. Less than 20-ns amplification delay.

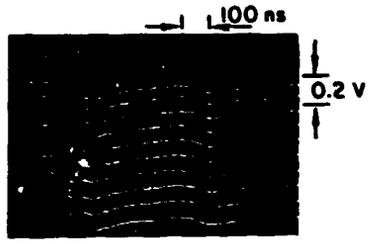

(a) RECEIVER FIELD STOP 3

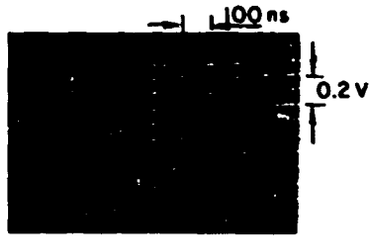

(b) RECEIVER FIELD STOP 1

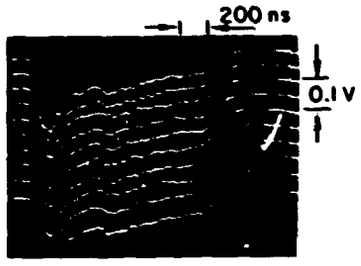

(c) RECEIVER FIELD STOP 1. White target lowered in water.

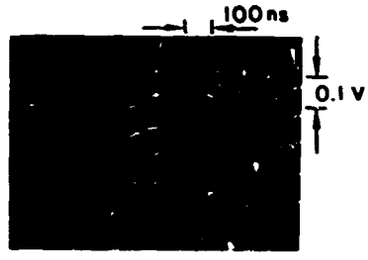

(d) RECEIVER FIELD STOP 1. White target lowered in water.

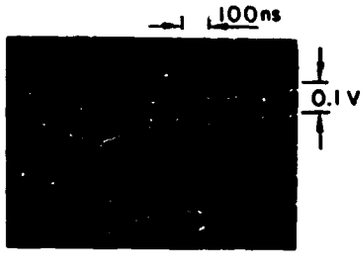

(e) RECEIVER FIELD STOP 1. Target out of view except for one return.

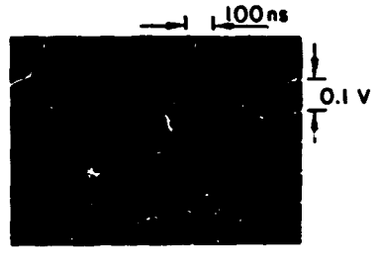

(f) RECEIVER FIELD STOP 2. Target out of view.

TA-7325-22

FIGURE 23 LIDAR RETURNS UNDER WATER OFF MONTEREY, 22 AUGUST 1969. Less than 20-ns amplification delay.

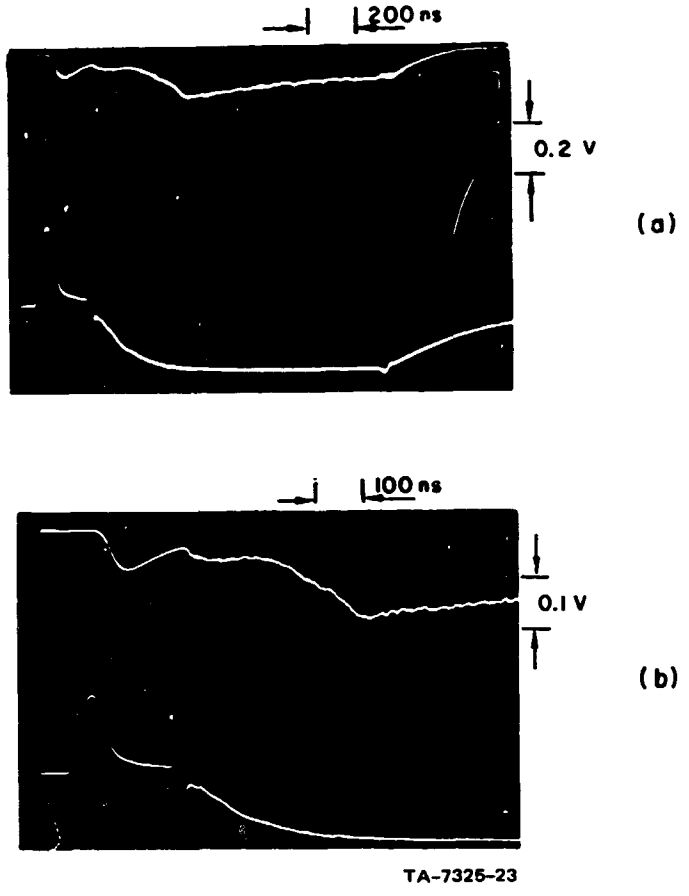

FIGURE 24 LIDAR RETURNS UNDER WATER OFF MONTEREY 22 AUGUST 1969. 200-ns amplification delay. Receiver Field Stop 2.

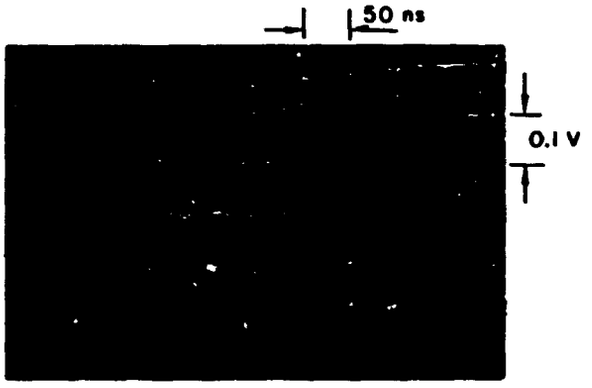

(a) RECEIVER FIELD STOP CLOSED. Signal indicates amplification "turn on" at about 175 ns.

(b) RECEIVER FIELD STOP 4. Signal begins at about 150 ns.

TA-7326-24

FIGURE 25 LIDAR RETURNS UNDER WATER OFF MONTEREY, 22 AUGUST 1969. Less than 20-ns amplification delay.

fiber-optic guide, between the actual laser emission from the transmitter and the monitor pulse, which is the PIN diode output. Only the latter is recorded by the scope in the lower trace. This small delay is ignored in the discussion.) In Figure 24, the following three distinct stages are seen. First, the PMT response to the overloading signal is seen when the gain of the PMT is very low (as much as -60 dB below the "turned on" condition, depending on dark current level). Secondly, the crosstalk referred to earlier accompanies the "turn on" pulse whose start is signalled by the sharp transient in the lower trace. Finally, as the PMT gain is restored, the afterpulse appears as an amplified signal. Figure 25(a) shows the crosstalk accompanying the "turn on" with the receiver closed, and Figure 25(b) shows the PMT signal with the receiver open. In these cases, delay before "turn on" is less than 20 ns. Comparison of these traces shows that with the receiver open, the PMT signal starts about 25 ns ahead of the "turn on" pulse.

Some further observations may be made by a comparison of Figure 18 (a) and (b), and Figure 24(a) and (b). The former, as will be recalled, are the traces produced when the PMT was overloaded by the sample of the laser pulse. It will be noted that the initial current pulses when the PMT gain is "turned down" have different amplitudes and rise times.

Though the monitor pulse (an indicator of the outgoing laser pulse) is much larger in Figure 24(a), the PMT pulse is smaller. It also rises slower and has a slightly longer delay after the monitor pulse than the corresponding pulse in Figure 18. Further, the afterpulses also differ in shape. In Figure 18, with a pulse overload, the afterpulse has a relatively sharp peak, whereas in Figure 24(a) and (b) the afterpulse appears stretched out.

The above observations lead to the following conclusions about the nature of the initial overloading signal. This signal does not arise

within the system. It begins within a few nanoseconds after the laser emission, ostensibly in the first few feet of water. Its intensity is lower than that of the laser sample, which is a 10-to-15-ns pulse with a total energy on the order of 10^{-6} joule. The duration of the overloading signal is longer than the laser pulse, as indicated by the signal as well as the stretched-out afterpulse. Either the power level or the total energy received during this longer interval is sufficient to cause overloading of the PMT.

It is evident that returns from single scattering events can be seen only after the transmitted beam and the receiver field of view have started to overlap. On reference to Table II, the overlap is seen to begin at 147, 90, 51, and 27 feet, respectively, for the field stops 1 through 4. With no multiple scattering, no signal should be seen till after about 430, 275, 170, and 104 ns, respectively (using a 30-ns delay for the PMT). Narrow-angle forward scattering can explain the target returns seen in Figure 23 at about 200 ns, a range of 70 feet. However, the only source of signals received within the first $\approx$20 ns after pulse emission that appears reasonable is the laser radiation multiply scattered at wide angles within a few meters of the lidar. Precise calculation of multiple scattering phenomena is complex and time-consuming, and requires data not available from these tests--viz., the value of the absorption coefficient, the value of the scattering coefficient, and the volume scattering function of the water in which the tests were made. However, order-of-magnitude calculations show that multiple wide-angle scattering may in fact have caused $\approx 10^{-2}$ watts to have been scattered into the receiver within the first 20 ns under the conditions prevailing during the tests.

Let us now turn our attention from the afterpulse problem to the details of the returns over the major portion of the lidar's range.

Consecutive returns from pulses at repetition intervals of about 15 seconds show differences in fine structure. The performance of the photomultiplier tube has apparently not been impaired by the overload except for the presence of the afterpulse, so differences in fine structure of the signal are apparently due to small turbidity changes in the water. Such turbidity changes can be expected to occur due to changes in the distribution of suspended particles resulting from wave motion; some signal differences may also result from the movement of the lidar.

In the absence of corroborative data on the ocean environment, additional interpretation of the traces is difficult at this stage.

V SUGGESTIONS FOR FUTURE WORK

From the foregoing, it is seen that good system performance is within easy reach. The only significant difficulty remaining is the initial overloading of the photomultiplier due to multiple wide-angle scattering.

Several practical fixes readily suggest themselves. The present 13-inch bistatic separation of the transmitter and receiver could be much increased to attenuate the early multiple scattering returns. Alternatively or additionally, a block could be placed in the path of the multiple wide-angle scattering; for example, a tube a few feet long could be attached to the transmitter to eliminate early multiple scattering returns. With these simple modifications the system can be readied for ocean turbidity-measurement work.

The overloading can probably also be eliminated by electronic means, if desired, and overloading can be prevented altogether by the use of an electro-optic shutter in front of the PMT.

The instrument is essentially ready for open-ocean operation. System calibration using in situ turbidity measurements is the logical next step. When calibration is completed, the lidar will be operational and available for open-ocean turbidity measurements.

VI SUMMARY AND CONCLUSION

The report describes the design, development, and evaluation of a high-sensitivity receiver and the upgrading of a laser transmitter for an underwater optical radar (lidar) system.

The laser system consists of a Q-switched Neodymium-doped glass laser whose output at 1062 nm is frequency-doubled by a KDP crystal to produce 531-nm radiation, which has near-minimum attenuation[2] in water. The output of the laser transmitter consists of pulses, 12 to 15 ns in length, about 15 millijoules in total energy, providing a peak power of about a megawatt in the green.

The receiver package is built around a high-performance photomultiplier tube and employs both amplitude-dependent and time-dependent video-gain-compression techniques in order to be able to display as large a dynamic range of signal amplitude as possible. Range-attenuation control is achieved through dynode-potential modulation. During standby the receiver gain is greatly reduced by operating with dynode potentials removed from the optimum values. The transmitted laser signal is used to trigger restoration of the optimum potentials in a manner that allows control of the rate and time of achievement of maximum gain. The signal from the anode of the photomultiplier is further processed by a logarithmic amplifier before video display in order to further compress the large dynamic range of the signal. The lidar receiving system has a bandwidth and a working speed compatible with the laser transmitter pulses. It is believed the system is capable of a range resolution of at least 2 meters and of detecting changes on the order of 10 to 15 percent in turbidity levels, depending on the range.

Three field trials of the system were made in the Pacific Ocean. The experience gained during these tests was used in greatly improving the system. The performance of the system has been sufficiently encouraging to strongly justify further extensive tests in various typical ocean environments.

The data collected to date indicates that even in relatively clear water, multiple wide-angle scattering close to the system provides a signal sufficiently strong to generate a temporary overload transient in the photomultiplier. In spite of this difficulty, the return over the major part of the range shows interesting detail and structure in the backscattering that probably can be correlated with variations in salinity, temperature, absorption, or attenuation. Use of the system in various ocean environments, in which the additional parameters can be measured simultaneously, is urgently needed to demonstrate the potential of this technique to accurately measure the turbidity structural characteristics and turbidity change characteristics of real ocean waters.

REFERENCES

1. G. P. Sorenson, R. C. Honey, and R. W. Gates, "Analysis of the Use of Airborne Laser Radar for Detecting Sub-Surface Submarine-Induced Turbidity Wakes (U)," Final Report, Contract N 62269-67-C-0403, SRI Project 6584, Stanford Research Institute, Menlo Park, Calif. (December 1967), SECRET (AD-389 803L).

2. G. L. Clarke and H. R. James, "Laboratory Analysis of the Selective Absorption of Light by Sea Water," J. Opt. Soc. Am., Vol. 29, pp. 43-55 (1939).

3. N. G. Jerlov, Optical Oceanography, p. 51 (Elsevier Publishing Company, New York, 1968).

4. J. A. Curcio and C. C. Petty, J. Opt. Soc. Am., Vol. 41, p. 302 (1951).

5. P. E. Gray, D. DeWitt, A. R. Boothroyd, and J. F. Gibbons, Physical Electronics and Circuit Models of Transistors (John Wiley & Sons, New York, 1964).

6. J. L. Stuart, "Solid State Logarithmic Amplifiers," JPL Space Programs Summary No. 37-18 (1965).

7. J. L. Stuart, "Logarithmic Amplifier Uses Field Effect Transistors," NASA Tech. Brief No. 65-10145 (1965).

8. R. L. Slice, "A Solid-State Logarithmic Video Amplifier for Pulse Applications," NRL Report No. 6147 (August 11, 1964).

UNCLASSIFIED
Security Classification

DOCUMENT CONTROL DATA - R & D

(Security classification of title, body of abstract and indexing annotation must be entered when the overall report is classified)

1. ORIGINATING ACTIVITY (Corporate author)

Stanford Research Institute
Menlo Park, California

2a. REPORT SECURITY CLASSIFICATION

Unclassified

2b. GROUP

3. REPORT TITLE

DEVELOPMENT OF A TURBIDITY-MEASURING UNDERWATER OPTICAL RADAR SYSTEM

4. DESCRIPTIVE NOTES (Type of report and inclusive dates)

Final Report Covering the period 1 June 1968 to 31 August 1969

5. AUTHOR(S) (First name, middle initial, last name)

Kamala S. Krishnan William E. Evans Richard C. Honey Glenn P. Sorenson

6. REPORT DATE	7a. TOTAL NO. OF PAGES	7b. NO. OF REFS
December 1969	78	8

8a. CONTRACT OR GRANT NO	9a. ORIGINATOR'S REPORT NUMBER(S)
N00014-68-C-0450	Final Report
b. PROJECT NO.	SRI Project 7325
c.	9b. OTHER REPORT NO(S) (Any other numbers that may be assigned this report)
d.	

10. DISTRIBUTION STATEMENT

11. SUPPLEMENTARY NOTES	12. SPONSORING MILITARY ACTIVITY
	Office of Naval Research Department of the Navy Washington, D.C.

13. ABSTRACT

The results of a feasibility study of measuring subsurface turbidity in the ocean are presented. The design and development of the laser transmitter and receiver packages of an underwater optical radar system are discussed. The initial performance of the equipment in three field trials in the Pacific Ocean is described, the data obtained is discussed, and the system is evaluated.

DD FORM 1 NOV 65 1473 (PAGE 1)

S/N 0101-807-6801

Unclassified
Security Classification

14 KEY WORDS	LINK A		LINK B		LINK C	
	ROLE	WT	ROLE	WT	ROLE	WT
Oceanographic studies						
Optical radar system						
Turbidity measurement						
Laser radar (lidar)						
Remote sensing						